
No Representation, No Trust: Connecting Representation, Collapse, and Trust Issues in PPO

Skander Moalla
skander.moalla@epfl.ch
CLAIRE, EPFL

Andrea Miele
CLAIRE, EPFL

Razvan Pascanu
Google DeepMind

Caglar Gulcehre
caglar.gulcehre@epfl.ch
CLAIRE, EPFL

Abstract

Reinforcement learning (RL) is inherently rife with non-stationarity since the states and rewards the agent observes during training depend on its changing policy. Therefore, networks in deep RL must be capable of adapting to new observations and fitting new targets. However, previous works have observed that networks in off-policy deep value-based methods exhibit a decrease in representation rank, often correlated with an inability to continue learning or a collapse in performance. Although this phenomenon has generally been attributed to neural network learning under non-stationarity, it has been overlooked in on-policy policy optimization methods which are often thought capable of training indefinitely. In this work, we empirically study representation dynamics in Proximal Policy Optimization (PPO) on the Atari and MuJoCo environments, revealing that PPO agents are also affected by feature rank deterioration and loss of plasticity. We show that this is aggravated with stronger non-stationarity, ultimately driving the actor’s performance to collapse, regardless of the performance of the critic. We ask why the trust region, specific to methods like PPO, cannot alleviate or prevent the collapse. We find that there is a connection between representation collapse and the degradation of the trust region, one exacerbating the other, and present Proximal Feature Optimization (PFO), a novel auxiliary loss that, along with other interventions, shows that regularizing the representation dynamics improves the performance of PPO agents. Code and run histories are available at <https://github.com/CLAIRE-Labo/no-representation-no-trust>.

1 Introduction

Reinforcement learning (RL) agents are inherently subject to non-stationarity as the states and rewards they observe change during learning. Therefore, neural networks in deep RL must be capable of adapting to new inputs and fitting new targets. However, previous works have observed that value networks in off-policy value-based algorithms exhibit a decrease in the rank of their representations, termed feature rank, and a decrease in their ability to regress to arbitrary targets, called plasticity (Kumar et al., 2021; Lyle et al., 2022). Consequently, this decrease in representation fitness was often correlated with the value network’s inability to continue learning and adapting to new tasks, especially in sparse-reward scenarios. Although this phenomenon is more generally attributed to neural networks trained under non-stationarity (Lyle et al., 2023), it has been overlooked in on-policy policy optimization methods that are often thought capable of training indefinitely. In particular, Proximal Policy Optimization (PPO) (Schulman et al., 2017), one of the most popular policy optimization methods, introduces additional non-stationarity by making several minibatch updates over non-stationary data and by optimizing a surrogate loss depending on a moving policy. This raises the question of how much PPO agents are impacted by the same representation degradation attributed to non-stationarity. Igl et al. (2021) have shown that non-stationarity affects the generalization of PPO agents (learning speed when training episodes are very different otherwise performance at test

time on novel episodes) but does not prevent training, and no connection was made with the feature rank and plasticity measures used in the recent value-based works. One open question is why the trust region embedded in methods like PPO is not able to prevent the deterioration in policy, by constraining its movement. Our contributions are the following:

1. We provide the first study of feature rank and plasticity in policy optimization, revealing that PPO agents in the Arcade Learning Environment (Bellemare et al., 2013) and MuJoCo (Todorov et al., 2012) environments are subject to representation collapse.
2. We draw connections between representation collapse, performance collapse, and trust region issues in PPO, showing that PPO’s clipping becomes ineffective under poor representations and fails to prevent performance collapse, which is irrecoverable due to loss of plasticity.
3. We corroborate these connections by performing interventions that regularize non-stationarity and representations and result in a better trust region and mitigation of performance collapse, incidentally giving insights on sharing an actor-critic trunk.
4. We propose *Proximal Feature Optimization* (PFO), a new regularization on the representation of the policy that regularizes the change in pre-activations. By addressing the representation issues, PFO can mitigate performance collapse and improve the agent’s performance.
5. We open source our code and run histories, providing a comprehensive and reproducible codebase for studying representation dynamics in policy optimization and a large database of run histories with extensive logging for further investigation on this topic.

2 Background

Reinforcement Learning (Sutton & Barto, 2018) We formalize our RL setting with the finite-horizon undiscounted Markov decision process, describing the interaction between an agent and an environment with finite ¹ sets of states \mathcal{S} and actions \mathcal{A} , and a reward function $r : \mathcal{S} \times \mathcal{A} \times \mathcal{S} \rightarrow \mathbb{R}$. An initial state $S_0 \in \mathcal{S}$ is sampled from the environment, then at each time step $t \in \{0, \dots, t_{\max} - 1\}$, the agent observes the state $S_t \in \mathcal{S}$, picks an action $A_t \in \mathcal{A}$ according to its policy $\pi : \mathcal{S} \rightarrow \Delta(\mathcal{A})$ with probability $\pi(A_t|S_t)$, ² observes the next state $S_{t+1} \in \mathcal{S}$ sampled from the environment and receives a reward $R_{t+1} \doteq r(S_t, A_t, S_{t+1})$. We denote by $G_t \doteq \sum_{k=t}^{t_{\max}-1} R_{k+1}$ the return after the action at time step t . The goal of the agent is to maximize its expected return $J(\pi) \doteq \mathbb{E}_{\pi} \left[\sum_{t=0}^{t_{\max}-1} R_{t+1} \right] = \mathbb{E}_{\pi} [G_0]$ over the induced random trajectories. We discuss the choice of this setting in Appendix A.1.

Actor-Critic Agent We consider on-policy deep actor-critic agents which train a policy (or actor) network $\pi(\cdot; \theta)$ also denoted π_{θ} , and a value (or critic) network $\hat{v}(\cdot; \mathbf{w})$ that approximates the return of π_{θ} at every state. At every training stage, the agent collects a batch of samples, called rollout, with its current policy π_{θ} , and both networks are trained with gradient descent on this data. The critic is trained to minimize the Euclidean distance to an estimator of the returns (e.g., G_t). We use λ -returns computed with the Generalized Advantage Estimator (GAE) (Schulman et al., 2015b). The actor is trained with the Proximal Policy Optimization (PPO) (Schulman et al., 2017).

Proximal Policy Optimization PPO-Clip, the most popular variant of PPO algorithms proposed by Schulman et al. (2017), optimizes the actor by maximizing the objective in Equation 1 at each rollout.

$$L_{\pi_{\text{old}}}^{CLIP}(\theta) = \mathbb{E}_{\pi_{\text{old}}} \left[\sum_{t=0}^{t_{\max}-1} \min \left(\frac{\pi_{\theta}(A_t|S_t)}{\pi_{\text{old}}(A_t|S_t)} \Psi_t, \text{clip} \left(\frac{\pi_{\theta}(A_t|S_t)}{\pi_{\text{old}}(A_t|S_t)}, 1 + \epsilon, 1 - \epsilon \right) \Psi_t \right) \right] \quad (1)$$

The objective is defined for some small hyperparameter ϵ , where π_{old} is the last π_{θ} of the previous optimization stage. It is used to collect the training batch, and Ψ_t is an estimator of the advantage of π_{old} (e.g., $\Psi_t = G_t - \hat{v}(S_t; \mathbf{w}_{\text{old}})$); we use the GAE in our experiments. The objective is optimized

¹The pixel-based environment with discrete actions used in our experiments and our simple theoretical example in Section 3.2.1 fit the finite state and action formalism but not our continuous action space environment. We refer the reader to Szepesvári (2022) for a formalism of RL in that setting.

²The time step t is included in the representation of S_t to preserve the Markov property in finite-horizon tasks as done by Pardo et al. (2018) and is analogous to considering time-dependent policies in the classical formulation of finite-horizon MDPs.

with minibatch gradient steps over multiple epochs on the rollout data (batch). We refer to PPO-Clip as PPO and provide a high-level pseudocode in Algorithm 1.

Intuitively, PPO aims to maximize the policy advantage $\mathbb{E}_{\pi_{\text{old}}}\left[\sum_{t=0}^{t_{\text{max}}-1} \frac{\pi_{\theta}(A_t|S_t)}{\pi_{\text{old}}(A_t|S_t)} \Psi_t\right]$ defined by Kakade & Langford (2002), which participates in a lower bound to the improvement of π_{θ} given that it is close to π_{old} (Schulman et al., 2015a, see Theorem 1). In this regard, a gradient step on $L_{\pi_{\text{old}}}^{\text{CLIP}}(\theta)$ would increase (decrease) the probability of actions at states yielding positive (negative) advantage until the ratio between the policies for those actions reaches $1 + \epsilon(1 - \epsilon)$ at which point the gradient at those samples becomes null. This is a heuristic to ensure a trust region that keeps policies close to each other, resulting in policy improvement.

Non-stationarity in deep RL and PPO The actor and the critic networks are both subject to non-stationarity in deep RL. As the agent improves, it visits different states, shifting the distribution of states which makes the networks’ input distribution non-stationary. This also holds for the targets to fit the critic, which change as the policy returns change. This form of non-stationarity has been shown by previous work to hinder the ability of several deep RL agents (e.g., DQN (Mnih et al., 2015), SAC (Haarnoja et al., 2018)) to continue learning (Lyle et al., 2022; Nikishin et al., 2022). PPO introduces additional non-stationarity to the actor compared to policy gradient methods (such as vanilla policy gradient (Sutton et al., 1999), A2C Mnih et al. (2016)). Its objective is non-stationary as it depends on the previous policy and it is optimized by performing multiple epochs of minibatch gradient descent on every new collected batch, making the networks more likely to be impacted by previous training rollouts as new rollouts are collected. Increasing the number of epochs can cause the agent to “overfit” more to previous experience, making the impact of non-stationarity stronger.

Feature rank As done in most works studying feature dynamics in deep RL (Lyle et al., 2022; Kumar et al., 2021), we refer to the activations of the last hidden layer of a network (the penultimate layer) as the features or representation learned by the network. On a batch of N samples, this gives a matrix of dimensions $N \times D$ denoted by Φ , where $D < N$ is the width of the penultimate layer. Several measures of the rank of this matrix have been used to quantify the “quality” of the representation (Kumar et al., 2021; Gulcehre et al., 2022; Lyle et al., 2022; Andriushchenko et al., 2023). Their absolute values differ significantly, but their dynamics are often correlated. We track all of the different rank metrics in our experiments, compare them in Appendix E, and use the *approximate rank* in our main figures for its connection to principal component analysis (PCA). Given a threshold $\delta \in \mathbb{R}$ and the singular values $(\sigma_1(\Phi), \dots, \sigma_D(\Phi))$ of Φ in decreasing order, the approximate rank of Φ is $\min_k \left\{ \frac{\sum_{i=1}^k \sigma_i^2(\Phi)}{\sum_{j=1}^D \sigma_j^2(\Phi)} > 1 - \delta \right\}$ which corresponds to the smallest dimension of the subspace recovering $(1 - \delta)\%$ of the variance of Φ . We use $\delta = 0.01$ i.e. the reconstruction recovers 99% of the variance as done by Andriushchenko et al. (2023); Yang et al. (2020). We refer to this metric as *feature rank* with reference to the rank of the *feature* matrix when there is no ambiguity.

Plasticity loss Plasticity is computed on checkpoints of a network undergoing some training to measure the evolution of its ability to fit targets. Given a fixed target and a fixed optimization budget (number of gradient steps), a checkpoint’s plasticity loss is the loss from fitting the checkpoint to the target at the end of the optimization budget. Usually, the plasticity of a deep RL agent throughout training is measured by its ability to fit the outputs of a model initialized from the same distribution as the agent on a fixed rollout collected by this target random model (Lyle et al., 2022; Nikishin et al., 2023). The data would, in expectation, be from the same distribution as the agent’s initial checkpoint. To fit the critic, we use an L^2 loss on the outputs of the models. To fit the actor, we use a KL divergence between the target and the checkpoint (forward KL).

3 Deteriorating representations, collapse, and loss of trust

It is well-known that non-stationarity in deep RL can be a factor causing issues in representation learning. However, most of the observations have been made in value-based methods showing that value networks are prone to rank collapse, harming their expressivity, and in turn, the performance of the agent (Lyle et al., 2022; Kumar et al., 2022); Igl et al. (2021) studied non-stationarity in PPO but only showed that it harms its generalization, with no evidence of rank deterioration or performance collapse. Our motivation is to reuse the tools that showed that value-based methods are prone to representation collapse but in policy optimization methods for the first time. We focus on PPO for its popularity and extra non-stationarity through multi-epoch optimization. One open question,

compared to most value-based alternatives, is how the regularization implicit in PPO through its trust region interacts with this phenomenon. Intuitively it should prevent rapid degradation of the policy.

Experimental setup We begin our experiments by training PPO agents on the Arcade Learning Environment (ALE)(Bellemare et al., 2013) for pixel-based observations with discrete actions and on MuJoCo (Todorov et al., 2012) for continuous observations with continuous actions. To keep our experiments tractable, we choose the Atari-5 subset recommended by Aitchison et al. (2023) and add Gravitar to include at least one sparse-reward hard-exploration game from the taxonomy presented by Bellemare et al. (2016). For MuJoCo, we train on Ants, Half-Cheetahs, Humanoids, and Hoppers, which have varying complexity and observation and output sizes. We use the same model architectures and hyperparameters as popular implementations of PPO on ALE and MuJoCo (Raffin et al., 2021; Huang et al., 2022b); these are also the architectures and hyperparameters used by Schulman et al. (2017) in the original implementation of PPO; they do not include normalization layers. The ALE model uses ReLU activations (Nair & Hinton, 2010) and the MuJoCo one tanh; we also experiment with ReLU on MuJoCo. We use separate actor and critic models for both environments unless specified in Section 4. Details on the performance metrics and tables of all environment parameters, model architectures, and algorithm hyperparameters are presented in Appendix B. Observing that the previous findings on the feature dynamics of value-based approaches (Gulcehre et al., 2022; Lyle et al., 2022) apply to the critic of PPO as well since the loss function is the same, we focus on studying the feature dynamics of the actor unless stated otherwise in the text or figures.

We vary the number of epochs as a way to control the effect of non-stationarity, which gives the agent a more significant number of optimization steps per rollout while not changing the optimal target it can reach due to clipping, as opposed to changing the value of ϵ in the trust region for example. We keep the learning rate constant throughout training and use the same value for all the epoch configurations. To understand the feature dynamics, we measure different metrics that are proposed in the literature, including feature rank, number of dead neurons (Gulcehre et al., 2022), plasticity loss (Lyle et al., 2022), and penultimate layer pre-activation norm. Previous work has monitored feature norm values as well (Lyle et al., 2024); however, in our case, we found that as the neurons in the policy network die, the feature norm might be stable while the pre-activation norm blows up. All the metrics are computed on on-policy rollouts except for the plasticity loss.

We run five seeds per hyperparameter configuration and report mean curves with min/max shaded regions unless specified otherwise. All curves, except for plasticity loss, are smoothed using an exponentially weighted moving average with a coefficient of 0.05. We explore the following questions: **Q1.** How do a PPO agent’s representation metrics, such as the *feature rank* and the *plasticity loss*, evolve during training? Are they subject to the same decline observed by Kumar et al. (2021); Lyle et al. (2022) in value-based methods? Does it affect performance? **Q2.** How does increasing the number of epochs per rollout to vary non-stationarity affect a PPO agent’s representation? Does it degrade as observed in DQN and SAC agents when increasing the replay ratio (Nikishin et al., 2022; Kumar et al., 2022)?

3.1 PPO suffers from deteriorating representations

Q1. Deteriorating representation As illustrated in Figure 1 with ALE/Phoenix as an example, we observe a consistent increase in the norm of the pre-activations of the feature layer of the policy network. Learning curves for all the ALE games and MuJoCo tasks considered can be found in Appendix D. The increase in feature norm is present in all the games/tasks considered in both environments, that is, with the two different model architectures and activation functions in the case of MuJoCo. We associate the rapid growth in the norm of the pre-activations with an eventual decline in the policy network’s feature rank. We observe a rank decline in five out of six ALE games and seven out of eight MuJoCo tasks (four with ReLU and three with tanh). The same observations about the increasing norm of the pre-activations can be made about the critic network. However, its rank varies more with the sparsity of the reward. In most environments, its rank experiences a significant deterioration after the policy’s performance (not its rank) declines and rewards become sparser. In the sparse-reward game Gravitar, the critic’s rank collapses before the policy. Furthermore, plasticity loss is increasing for the critic, as observed in value-based plasticity studies and it is also the case for the actor, for which it explodes around rank collapse.

Q2. Worse consequences Increasing the replay ratio in DQN and SAC deteriorates the agent’s representation and, in turn, its performance (Kumar et al., 2022; D’Oro et al., 2023). This is commonly attributed to “overfitting” to previous experience (Nikishin et al., 2022). Increasing the number of

epochs in PPO is analogous, and a natural hypothesis is that this would accelerate the deterioration of the policy’s representation. Figure 1 shows that increasing the number of epochs accelerates the increase of pre-activations norm and the decrease of the policy’s feature rank. In some cases, the rank eventually collapses, coinciding with a policy’s performance collapse. We observe the performance collapse in three of the six ALE games and three of the four MuJoCo tasks.

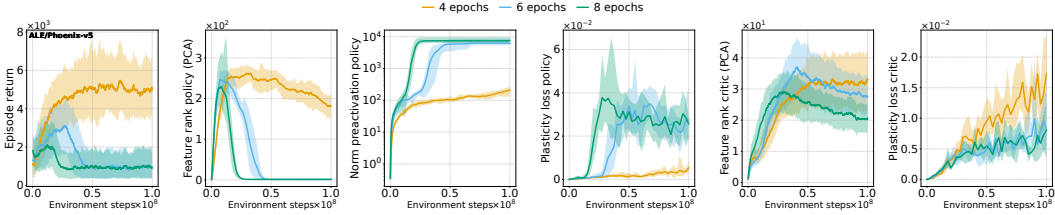


Figure 1: Deteriorating performance and representation metrics The policy network of a PPO-Clip agent on ALE/Phoenix-v5 is subject to a deteriorating representation. The norm of the pre-activations of the penultimate layer consistently increases, and its rank eventually decreases. Performing more optimization epochs per rollout to increase the effects of non-stationarity accelerates the growth of the norm of the pre-activations and the collapse of its rank. This ultimately leads to the collapse of the policy. This collapse is not driven by the value network, whose rank is still high.

Characterizing the collapse The collapse observed in the policy’s representation differs from the typical entropy collapse. As one can observe from Figure 2, the collapse in representation gives a policy that has high entropy (still lower than a uniform policy and its initialization). However, in MDPs, entropy is computed as the average across states. A high overall entropy can come from an average of high-entropy states with different action distributions or trivially from the same high-entropy distribution in all states. In our case, it is the latter: we compute the policy variance across states and observe that it collapses to zero, indicating that the policy network outputs the same action distribution at every state, which is often close to uniform. This is consistent with the policy representation, which has collapsed to a layer with mostly dead neurons³. The output layer gives the output distribution based on only the bias term, as the linear weights are multiplied by a null feature vector. Such a policy takes the same actions across all states; therefore, performance for non-trivial tasks would collapse.

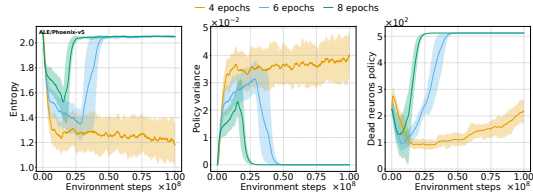


Figure 2: Rank collapse gives a high but trivial entropy The rank collapse of the policy gives a policy with high entropy but zero variance across states. The network outputs the same high-entropy action distribution in all states, as all the neurons in the feature layer are dead. Its output only depends on the constant bias term.

3.2 Collapsed representations create trust issues and unrecoverable loss

Intuitively, the heuristic trust region set by PPO-Clip should prevent sudden catastrophic changes and limit the rank collapse, which induces worse performance. However, empirically, it seems the trust region cannot mitigate the collapse. In this section, we seek to understand the interaction between the rank collapse and the trust region. We argue that as rank collapses, the clipping constraint becomes unreliable and unable to restrict learning. This is in line with previous works that have pointed out that probability ratios during training can go beyond the clipping limits with PPO-Clip (Engstrom et al., 2020; Wang et al., 2020; Sun et al., 2022). We believe, however, that this behavior is systematic when rank collapses and does not merely happen occasionally.

Wang et al. (2020, Theorem 2) state that when the gradients of the unclipped samples align with the gradients of clipped samples, the clipped samples’ ratios will have their probabilities continue to go beyond the clip limit. They claim this condition would hold in practice because of “optimization tricks” or optimizer accumulated moments; however, there is no evidence that these factors induce the gradient alignment or that the alignment is present in practice. Our intuition is that representation

³We consider a ReLU neuron as dead when its values are zero for all the samples in the batch and a tanh neuron dead when its standard deviation across samples is less than 0.001.

degradation leads to alignment in the gradients and, therefore, a breakdown of the trust region constraint. This can create a snowball effect, preventing PPO-Clip from preventing representation collapse. We summarize this in two observations:

1. Loss of trust is extreme around poor representations The average of probability ratios outside the clipping limits (below $1 - \epsilon$ in Figure 3) significantly diverges from the clipping limit around the collapse of the agent’s representation. This gives one more reason why the PPO trust region can be violated. We isolate this in a toy setting and analyze it formally in the next section. We further show in Figure 4 scatter plots of the lowest average probability ratios in runs with their associated representation metrics (20 points per run, across windows of size 1% training progress, spanning at least the horizon of the environment, so that points are well spaced in the run, with each point being the average of the window); we observe no significant correlation in the regions where the representation is rich (high rank, low pre-activation norm), but an apparent decrease of the average of probability ratios below $1 - \epsilon$ is observed as the representation reaches poor values.

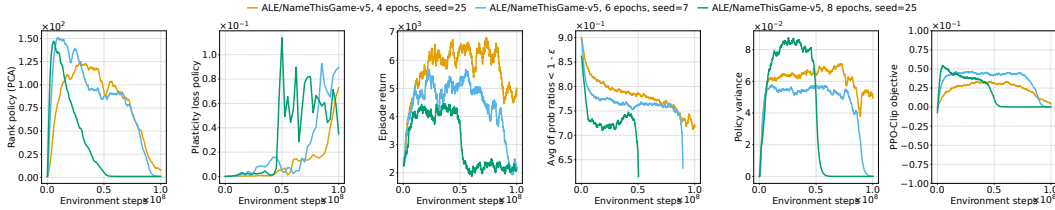


Figure 3: **Focusing on individual runs** Individual training curves on ALE/NameThisGame-v5 with different epochs per batch. Extremely low ratios are observed around the representation collapse of a PPO-Clip agent, implying that the heuristic trust region breaks down when representation power is lacking. The last-minibatch value of the PPO objective decreases towards 0 around the representation collapse, implying a reduction in the ability to improve the policy and recover, which is corroborated by the increase in plasticity loss. (Ratios are trivially above $1 - \epsilon$ after collapse as a collapsed model does not change much to have values below $1 - \epsilon$.)

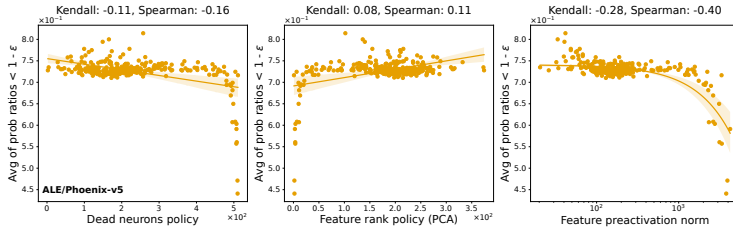


Figure 4: **Representation vs trust region** Samples from ALE/Phoenix-v5 training curves. Each point maps an average of the probability ratios below the clipping limit vs. its corresponding average representation metric (dead neurons, feature rank, feature norm). The average ratios are significantly lower around poor representations (high dead neurons, low policy rank, high feature norm) reflecting the failure of the trust region. Averages are over non-overlapping windows larger than episodes.

2. Loss of plasticity renders performance collapse unrecoverable The persistent decrease in performance overlaps with a monotonic decrease in policy variance and PPO objective. It appears that as the policy loses its ability to distinguish state, it can also ascend the PPO objective less and less at each batch (recall: after collecting a batch, the loss starts around zero with a normalized advantage, and through minibatch updates, the clipped policy advantage is ascended). Intuitively, this is implied by a loss of plasticity or a collapse in entropy (no new actions to learn from). As seen in Section 2 the entropy does not collapse, and measuring the plasticity loss in Figure 3 shows that the decrease in objective gain is associated with a significant increase in plasticity loss.

Connecting the dots Hence, around collapse, the representation of the policy is getting so poor that it is impacting its ability to distinguish and act differently across states; the trust region cannot prevent this catastrophic change as it also breaks down with a poor representation; finally, the policy’s plasticity is also becoming so poor that the agent cannot recover by optimizing the surrogate objective.

3.2.1 A toy setting to understand the effects of rank collapse on trust region

We present a toy example that illustrates how a collapsed representation bypasses the clipping set by PPO and cannot satisfy the trust region it seeks to set. PPO constructs a trust region around the policy $\pi_\theta(\cdot|s)$ of the agent evaluated at a given state s , enforcing (in an approximate way) that the update computed on state s can not move the policy $\pi_\theta(\cdot|s)$ outside of the trust region. However, the constraint does not capture how updates computed on another state s' affect the policy's probability distribution over the current state s . The underlying assumption is that updates computed on different states are, at least in expectation, approximately orthogonal to each other, and they do not interact. Therefore, restricting the update of the current state is sufficient to keep the policy within the region.

In our case, however, one can show that as the rank collapses or the neurons die, the representations corresponding to different states become more colinear.⁴ Therefore, the gradients also become more colinear. In the extreme case, when the rank collapses to 1, or there is only one neuron alive, all representations are exactly colinear; therefore, all gradients are also. This means that even though clipping prevents the policy $\pi_\theta(\cdot|s)$ on the current state s from changing due to the update of that state $\nabla L(\pi_\theta(\cdot|s))$, $\pi_\theta(\cdot|s)$ will still change and move outside of the trust region due to the updates on other states s' . Leading to the trust region constraint being ineffective and not constraining the learning process in any meaningful sense. This gives a clear situation where the theorem of Wang et al. (2020) holds and can easily be analyzed as below without resorting to the theorem for an end-to-end proof or to get a better intuition.

Formal statement of the toy setting Let us consider a batch containing two state-action pairs (x, a_1) and (y, a_1) with sampled probabilities $\pi_{\text{old}}(a_1|x)$ and $\pi_{\text{old}}(a_1|y)$ and positive estimated advantages $A(x, a_1), A(y, a_1) > 0$. Let $\phi(x), \phi(y) \in \mathbb{R}$ be fixed 1-dimensional representations of x , and y that can be seen as the output of the (frozen) penultimate layer of a policy network with collapsed representation (all but one dead neuron), and let $\alpha \in \mathbb{R}$ such that $\phi(y) = \alpha\phi(x)$. Let $\theta = [\theta_1, \theta_2]$, be the last layer of the network, computing the logits of two actions, a_1 and a_2 , that are fed into a softmax to compute the probabilities. I.e., $\pi_\theta(a_i|s) = \frac{e^{\theta_1 \phi(s)}}{e^{\theta_1 \phi(s)} + e^{\theta_2 \phi(s)}}$. Consider PPO minibatch updates alternating between (x, a_1) and (y, a_1) . Ideally, the PPO loss increases $\pi_\theta(a_1|s)$ at gradients on (x, a_1) until it reaches the clip ratio and similarly on (y, a_1) . However, we show in Appendix C that a gradient step in (x, a_1) also affects $\pi_\theta(a_1|y)$ and depending on α will increase it past its clipped ratio, or decrease it below its initial value.

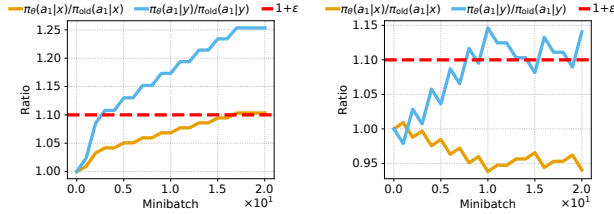


Figure 5: **Simulation of the toy setting** Left ($\alpha > 0$): a gradient on (x, a_1) takes the probability of (y, a_1) up and vice versa. When one is above the threshold and should not increase, the other still pushes it. Right ($\alpha < 0$): a gradient on (x, a_1) takes the probability of (y, a_1) down and vice versa. Both slow each down, with one forcing the other to be lower than its initial value.

Essentially, when $\alpha \geq 0$, a gradient on (x, a_1) increases θ_1^{new} therefore increasing both $\pi_{\theta^{\text{new}}}(a_1|x)$ and $\pi_{\theta^{\text{new}}}(a_1|y)$. The same holds for a gradient on (y, a_1) , causing one state to reach the clip limit first depending on $\alpha > 1$ but still have the other keep pushing its probability upwards. However, when $\alpha \leq 0$, a gradient on (x, a_1) increases θ_1^{new} therefore increasing $\pi_{\theta^{\text{new}}}(a_1|x)$ but decreasing $\pi_{\theta^{\text{new}}}(a_1|y)$. For a gradient on (y, a_1) it is the opposite: θ_1^{new} decreases therefore $\pi_{\theta^{\text{new}}}(a_1|x)$ decreases and $\pi_{\theta^{\text{new}}}(a_1|y)$ increases, causing each state to reduce the probability of the other, and depending on $\alpha < 1$ one of the probabilities will dominate and push the other one down. Figure 5 shows the evolution of the probabilities when simulating the updates empirically.

4 Intervening to regularize representations and non-stationarity

Having observed that PPO is affected by a frequent representation degradation that impacts its trust region heuristic and causes its performance to collapse, we turn to study interventions that aim at regularizing the representation of the policy network or reducing the non-stationarity in the optimization. We investigate whether these interventions improve the representation metrics we track and if in turn, this affects performance. We choose simple interventions that do not apply

⁴The expected angle between representations shrinks to 0.

modifications to the models during training (e.g., resetting or adding neurons) or require significantly more memory (e.g., maintaining separate copies of the models). We perform interventions on the games/tasks where the collapse is the most significant. We are interested in the state of the agent at the end of the training budget. We record the performance and representation metrics for each run as averages over the last 5% of training progress. We measure the excess ratio at a timestep as the average probability ratio above $1 + \epsilon$ divided by the average probability ratio below $1 - \epsilon$ at that timestep. This metric gives an idea of how much the policy exceeds the trust region. Its average value is computed over the last 5% of training progress where the ratios are non-trivial, giving the same window at the end of training as the other metrics when there is no collapse, otherwise a window before total collapse covering 5% of training progress, as after collapse, the model does not change anymore and the ratios are trivially within the $1 + \epsilon$ and $1 - \epsilon$ limits. We give additional details on the computation of these aggregate metrics and the interventions performed in Appendix B.

PFO: Regularizing features to mitigate trust issues The motivation for our first intervention and our proposed regularization method comes from our observation that the norm of the preactivation features is consistently increasing, which can be linked to the trust issues discussed in Section 3. We seek to mitigate this effect in a way that is analogous to the PPO trust region. We apply an L^2 loss on the difference between the pre-activated features of the optimized policy and the policy that collected the batch. This can also be thought of as a way to keep the pre-activations of the network during an update within a trust region. We apply this regularization to the pre-activations and not the activations, as dead neurons cannot propagate gradients, and even when they do, depending on the activation function, do so with a low magnitude. The regularization is an additional loss/penalty added to the overall loss. We term this loss the Proximal Feature Optimization (PFO) loss.

$$L_{\pi_{\text{old}}}^{\text{PFO}}(\theta) = \mathbb{E}_{\pi_{\text{old}}} \left[\sum_{t=0}^{t_{\text{max}}-1} (\phi_{\theta}(S_t) - \phi_{\text{old}}(S_t))^2 \right] \quad (2)$$

We apply two versions of PFO: one on only the penultimate layer’s pre-activations and one on all the pre-activations until the penultimate layer. In the scope of this work, we do not tune the coefficient of PFO; we pick the closest power of 10 that sets the magnitude of this loss to a similar magnitude of the clipped PPO objective tracked on the experiments without intervention. This gives a coefficient of 1 for ALE, 1 for MuJoCo with tanh, and 10 with ReLU. The goal is not necessarily to obtain better performance but to see if PFO improves the representations learned by PPO and if, in turn, it affects its trust region and performance. As shown in Figure 6, the regularization of PFO effectively brings the norm of the preactivation down, the number of dead neurons down, the plasticity loss down, and the rank up. This coincides with a significant decrease in the excess probability ratio, especially in the upper tail. More importantly, we also see a significant increase in the lower tail of the returns where no collapse in performance is observed anymore on ALE/NameThisGame and ALE/Phoenix, with a slight increase in the upper tail showing that PFO can increase performance. Among the interventions we have tried, PFO provided the most consistent improvements.

Sharing the actor-critic trunk In deep RL, the decision to use the same feature network trunk for both the actor and the critic is not trivial. Depending on the complexity of the environment, it can significantly vary the performance of a PPO agent (Andrychowicz et al., 2021; Huang et al., 2022a). We, therefore, attempt to draw a connection between sharing the feature trunk, the resulting representation, and its effects on the PPO objective. In this intervention, we make the actor and the critic share all the layers except their respective output layers and backpropagate the gradients from both the value and policy losses to the shared trunk. Figure 6 shows that the value loss acts as a regularizer, which decreases the feature rank and, depending on the reward’s sparsity, gives two distinct effects; In dense-reward environments such as ALE/Phoenix and ALE/NameThisGame, the ranks are concentrated at low but non-zero values: the upper tail significantly decreases compared to the baselines while the lower tail increases. This coincides with a lower feature norm, lower excess probability ratio, and, in turn, a high tail for the returns. It also increases performance in some cases. However, the opposite is true in the sparse-reward environment Gravitar: the rank completely collapses, and the feature norms and excess ratios are very high, collapsing the model’s performance. This is consistent with the observations made in the plasticity works studying value-based methods where sparse rewards deteriorate the rank of the value network. We provide training curves showing the difference in the evolution of the feature rank when sharing the actor-critic trunk in Appendix D.

Adapting Adam Asadi et al. (2023) argue that as the targets of the value function change with the changing policy rollouts, the old moments accumulated by Adam become harmful to fit the new

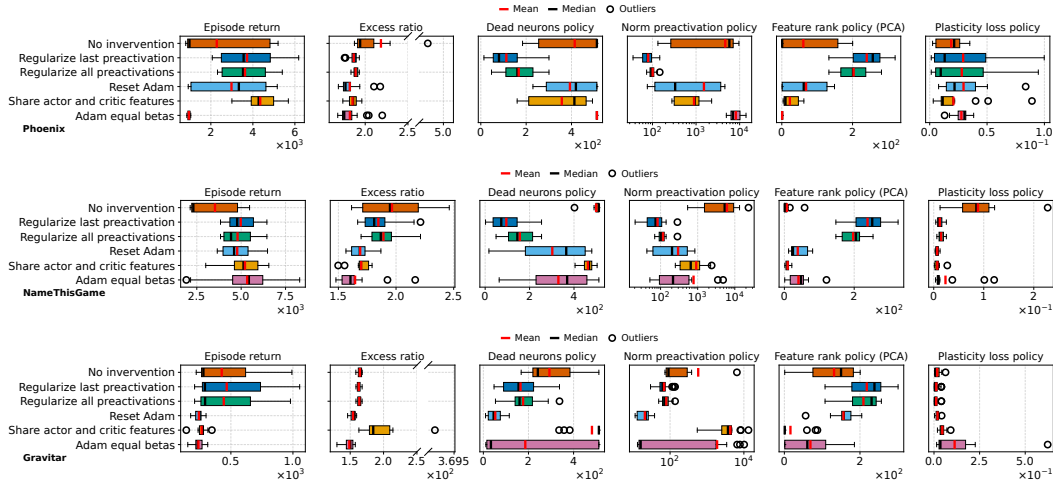


Figure 6: **Effects of regularizing features and non-stationarity** *Top: ALE/Phoenix-v5*. Regularizing the difference between the features of consecutive policies with PFO results in better representations and mitigates performance collapse while improving performance in some cases. *Bottom: ALE/Gravitar*. Sharing the feature trunk between the actor and the critic results in a worse policy representation as the value network is subject to rank collapse due to reward sparsity. A boxplot includes 15 runs with the different epochs.

targets and find that resetting the moments of Adam helps performance in DQN-like algorithms. As the PPO objective creates a dependency on the previous policy, and more generally, in the policy gradient, the advantages change with the policy, the same argument about Adam moments can be made for PPO. Furthermore, Dohare et al. (2023); Lyle et al. (2023) advocate for decaying the second moment of Adam faster than its default decay of 0.999 when training under non-stationarity and set it to match the decay of the first moment. Therefore, we experiment with both resetting Adam’s moments after each batch collection (to avoid tuning its frequency) and setting the second moment to decay at the (smaller) default decay of the first moment for both the actor and the critic; the moments are thus only accumulated over the epochs on the same batch in the former and over shorter batch sequences in the latter. We observe in Figure 6 and Appendix D that these interventions reduce the feature norm and increase the feature rank on ALE, which also reduces the excess probability ratio and, in some cases, improves performance; however, they are not sufficient to prevent collapse and, like sharing the actor-critic trunk, result in poor performance on ALE/Gravitar.

5 Conclusion and Discussion

Conclusion In this work, we have provided evidence that the representation deterioration under non-stationarity observed by previous work in value-based methods generalizes to PPO agents in ALE and MuJoCo with their common model architectures and can lead to performance collapse. We have shown that this is particularly concerning for the heuristic trust region set by PPO-Clip, which fails to prevent collapse as it becomes less effective when the agent’s representation becomes poor. Finally, we presented Proximal Feature Optimization (PFO), a simple novel auxiliary loss based on regularizing the features’ evolution that mitigates representation degradation and, along with other interventions, shows that controlling representation degradation improves performance.

Limitations and open questions In this work, we study the common architecture and optimizer of PPO agents in ALE and MuJoCo consisting of relatively small models without normalization layers, weight decay, or memory (e.g., not using Transformers and RNNs). Despite our best attempts, like any other empirical machine learning work, the generalization of our results to other settings is not fully known. Still, this work should raise awareness about the representation collapse phenomenon observed in PPO and encourage future work to monitor representations when training PPO agents, as it can help diagnose performance collapse. We have focused on interventions that regularize representations to highlight the connection between representation, trust region, and collapse, but exploring interventions on plasticity is also valuable as these may also influence the same dynamics. We believe further studies to analyze this problem, both empirically and particularly theoretically, to understand the reasons driving representation deterioration under non-stationarity to be valuable. We anticipate our study to encourage this.

References

- Matthew Aitchison, Penny Sweetser, and Marcus Hutter. Atari-5: Distilling the arcade learning environment down to five games. In Andreas Krause, Emma Brunskill, Kyunghyun Cho, Barbara Engelhardt, Sivan Sabato, and Jonathan Scarlett (eds.), *Proceedings of the 40th International Conference on Machine Learning*, volume 202 of *Proceedings of Machine Learning Research*, pp. 421–438. PMLR, 23–29 Jul 2023. URL <https://proceedings.mlr.press/v202/aitchison23a.html>.
- Maksym Andriushchenko, Dara Bahri, Hossein Mobahi, and Nicolas Flammarion. Sharpness-aware minimization leads to low-rank features. In A. Oh, T. Neumann, A. Globerson, K. Saenko, M. Hardt, and S. Levine (eds.), *Advances in Neural Information Processing Systems*, volume 36, pp. 47032–47051. Curran Associates, Inc., 2023. URL https://proceedings.neurips.cc/paper_files/paper/2023/file/92dd1adab39f362046f99dfe3c39d90f-Paper-Conference.pdf.
- Marcin Andrychowicz, Anton Raichuk, Piotr Stańczyk, Manu Orsini, Sertan Girgin, Raphaël Marinier, Leonard Hussenot, Matthieu Geist, Olivier Pietquin, Marcin Michalski, Sylvain Gelly, and Olivier Bachem. What matters for on-policy deep actor-critic methods? a large-scale study. In *International Conference on Learning Representations*, 2021. URL <https://openreview.net/forum?id=nIAxjsniDzg>.
- Kavosh Asadi, Rasool Fakoor, and Shoham Sabach. Resetting the optimizer in deep rl: An empirical study. In A. Oh, T. Neumann, A. Globerson, K. Saenko, M. Hardt, and S. Levine (eds.), *Advances in Neural Information Processing Systems*, volume 36, pp. 72284–72324. Curran Associates, Inc., 2023. URL https://proceedings.neurips.cc/paper_files/paper/2023/file/e4bf5c3245fd92a4554a16af9803b757-Paper-Conference.pdf.
- Marc Bellemare, Sriram Srinivasan, Georg Ostrovski, Tom Schaul, David Saxton, and Remi Munos. Unifying count-based exploration and intrinsic motivation. In D. Lee, M. Sugiyama, U. Luxburg, I. Guyon, and R. Garnett (eds.), *Advances in Neural Information Processing Systems*, volume 29. Curran Associates, Inc., 2016. URL https://proceedings.neurips.cc/paper_files/paper/2016/file/afda332245e2af431fb7b672a68b659d-Paper.pdf.
- Marc G Bellemare, Yavar Naddaf, Joel Veness, and Michael Bowling. The arcade learning environment: An evaluation platform for general agents. *Journal of Artificial Intelligence Research*, 47: 253–279, 2013.
- Albert Bou, Matteo Bettini, Sebastian Dittert, Vikash Kumar, Shagun Sodhani, Xiaomeng Yang, Gianni De Fabritiis, and Vincent Moens. TorchRL: A data-driven decision-making library for pytorch. In *The Twelfth International Conference on Learning Representations*, 2024. URL <https://openreview.net/forum?id=QxItoEAVMb>.
- Shibhansh Dohare, Qingfeng Lan, and A. Rupam Mahmood. Overcoming policy collapse in deep reinforcement learning. In *Sixteenth European Workshop on Reinforcement Learning*, 2023. URL <https://openreview.net/forum?id=m9Jfdz4ym0>.
- Pierluca D’Oro, Max Schwarzer, Evgenii Nikishin, Pierre-Luc Bacon, Marc G Bellemare, and Aaron Courville. Sample-efficient reinforcement learning by breaking the replay ratio barrier. In *The Eleventh International Conference on Learning Representations*, 2023. URL <https://openreview.net/forum?id=OpC-9aBBVJe>.
- Logan Engstrom, Andrew Ilyas, Shibani Santurkar, Dimitris Tsipras, Firdaus Janoos, Larry Rudolph, and Aleksander Madry. Implementation matters in deep rl: A case study on ppo and trpo. In *International Conference on Learning Representations*, 2020. URL <https://openreview.net/forum?id=r1etN1rtPB>.
- Caglar Gulcehre, Srivatsan Srinivasan, Jakub Sygnowski, Georg Ostrovski, Mehrdad Farajtabar, Matthew Hoffman, Razvan Pascanu, and Arnaud Doucet. An empirical study of implicit regularization in deep offline RL. *Transactions on Machine Learning Research*, 2022. ISSN 2835-8856. URL <https://openreview.net/forum?id=HFfJWx60IT>.

- Tuomas Haarnoja, Aurick Zhou, Kristian Hartikainen, George Tucker, Sehoon Ha, Jie Tan, Vikash Kumar, Henry Zhu, Abhishek Gupta, Pieter Abbeel, et al. Soft actor-critic algorithms and applications. *arXiv preprint arXiv:1812.05905*, 2018.
- Shengyi Huang, Rousslan Fernand Julien Dossa, Antonin Raffin, Anssi Kanervisto, and Weixun Wang. The 37 implementation details of proximal policy optimization. *The ICLR Blog Track 2023*, 2022a.
- Shengyi Huang, Rousslan Fernand Julien Dossa, Chang Ye, Jeff Braga, Dipam Chakraborty, Kinal Mehta, and João G.M. Araújo. Cleanrl: High-quality single-file implementations of deep reinforcement learning algorithms. *Journal of Machine Learning Research*, 23(274):1–18, 2022b. URL <http://jmlr.org/papers/v23/21-1342.html>.
- Minyoung Huh, Hossein Mobahi, Richard Zhang, Brian Cheung, Pulkit Agrawal, and Phillip Isola. The low-rank simplicity bias in deep networks. *Transactions on Machine Learning Research*, 2023. ISSN 2835-8856. URL <https://openreview.net/forum?id=bCiNWDmLY2>.
- Maximilian Igl, Gregory Farquhar, Jelena Luketina, Wendelin Boehmer, and Shimon Whiteson. Transient non-stationarity and generalisation in deep reinforcement learning. In *International Conference on Learning Representations*, 2021. URL <https://openreview.net/forum?id=Qun8fv4qSby>.
- Sham Kakade and John Langford. Approximately optimal approximate reinforcement learning. In *Proceedings of the Nineteenth International Conference on Machine Learning*, ICML '02, pp. 267–274, San Francisco, CA, USA, 2002. Morgan Kaufmann Publishers Inc. ISBN 1558608737.
- M. G. Kendall. A new measure of rank correlation. *Biometrika*, 30(1/2):81–93, 1938. ISSN 00063444. URL <http://www.jstor.org/stable/2332226>.
- Aviral Kumar, Rishabh Agarwal, Dibya Ghosh, and Sergey Levine. Implicit under-parameterization inhibits data-efficient deep reinforcement learning. In *International Conference on Learning Representations*, 2021. URL <https://openreview.net/forum?id=09bnihsFfXU>.
- Aviral Kumar, Rishabh Agarwal, Tengyu Ma, Aaron Courville, George Tucker, and Sergey Levine. DR3: Value-based deep reinforcement learning requires explicit regularization. In *International Conference on Learning Representations*, 2022. URL <https://openreview.net/forum?id=P0vMvLi91f>.
- Clare Lyle, Mark Rowland, and Will Dabney. Understanding and preventing capacity loss in reinforcement learning. In *International Conference on Learning Representations*, 2022. URL <https://openreview.net/forum?id=ZkC8wKoLbQ7>.
- Clare Lyle, Zeyu Zheng, Evgenii Nikishin, Bernardo Avila Pires, Razvan Pascanu, and Will Dabney. Understanding plasticity in neural networks. In Andreas Krause, Emma Brunskill, Kyunghyun Cho, Barbara Engelhardt, Sivan Sabato, and Jonathan Scarlett (eds.), *Proceedings of the 40th International Conference on Machine Learning*, volume 202 of *Proceedings of Machine Learning Research*, pp. 23190–23211. PMLR, 23–29 Jul 2023. URL <https://proceedings.mlr.press/v202/lyle23b.html>.
- Clare Lyle, Zeyu Zheng, Khimya Khetarpal, Hado van Hasselt, Razvan Pascanu, James Martens, and Will Dabney. Disentangling the causes of plasticity loss in neural networks. *arXiv preprint arXiv:2402.18762*, 2024.
- Marlos C Machado, Marc G Bellemare, Erik Talvitie, Joel Veness, Matthew Hausknecht, and Michael Bowling. Revisiting the arcade learning environment: Evaluation protocols and open problems for general agents. *Journal of Artificial Intelligence Research*, 61:523–562, 2018.
- Volodymyr Mnih, Koray Kavukcuoglu, David Silver, Andrei A Rusu, Joel Veness, Marc G Bellemare, Alex Graves, Martin Riedmiller, Andreas K Fidjeland, Georg Ostrovski, et al. Human-level control through deep reinforcement learning. *nature*, 518(7540):529–533, 2015.

- Volodymyr Mnih, Adria Puigdomenech Badia, Mehdi Mirza, Alex Graves, Timothy Lillicrap, Tim Harley, David Silver, and Koray Kavukcuoglu. Asynchronous methods for deep reinforcement learning. In Maria Florina Balcan and Kilian Q. Weinberger (eds.), *Proceedings of The 33rd International Conference on Machine Learning*, volume 48 of *Proceedings of Machine Learning Research*, pp. 1928–1937, New York, New York, USA, 20–22 Jun 2016. PMLR. URL <https://proceedings.mlr.press/v48/mniha16.html>.
- Vinod Nair and Geoffrey E Hinton. Rectified linear units improve restricted boltzmann machines. In *Proceedings of the 27th international conference on machine learning (ICML-10)*, pp. 807–814, 2010.
- Evgenii Nikishin, Max Schwarzer, Pierluca D’Oro, Pierre-Luc Bacon, and Aaron Courville. The primacy bias in deep reinforcement learning. In Kamalika Chaudhuri, Stefanie Jegelka, Le Song, Csaba Szepesvari, Gang Niu, and Sivan Sabato (eds.), *Proceedings of the 39th International Conference on Machine Learning*, volume 162 of *Proceedings of Machine Learning Research*, pp. 16828–16847. PMLR, 17–23 Jul 2022. URL <https://proceedings.mlr.press/v162/nikishin22a.html>.
- Evgenii Nikishin, Junhyuk Oh, Georg Ostrovski, Clare Lyle, Razvan Pascanu, Will Dabney, and Andre Barreto. Deep reinforcement learning with plasticity injection. In A. Oh, T. Neumann, A. Globerson, K. Saenko, M. Hardt, and S. Levine (eds.), *Advances in Neural Information Processing Systems*, volume 36, pp. 37142–37159. Curran Associates, Inc., 2023. URL https://proceedings.neurips.cc/paper_files/paper/2023/file/75101364dc3aa7772d27528ea504472b-Paper-Conference.pdf.
- Chris Nota and Philip S. Thomas. Is the policy gradient a gradient? In *Proceedings of the 19th International Conference on Autonomous Agents and MultiAgent Systems, AAMAS ’20*, pp. 939–947, Richland, SC, 2020. International Foundation for Autonomous Agents and Multiagent Systems. ISBN 9781450375184.
- Fabio Pardo, Arash Tavakoli, Vitaly Levдик, and Petar Kormushev. Time limits in reinforcement learning. In Jennifer Dy and Andreas Krause (eds.), *Proceedings of the 35th International Conference on Machine Learning*, volume 80 of *Proceedings of Machine Learning Research*, pp. 4045–4054. PMLR, 10–15 Jul 2018. URL <https://proceedings.mlr.press/v80/pardo18a.html>.
- William H. Press, Saul A. Teukolsky, William T. Vetterling, and Brian P. Flannery. *Numerical Recipes 3rd Edition: The Art of Scientific Computing*. Cambridge University Press, USA, 3 edition, 2007. ISBN 0521880688.
- Antonin Raffin, Ashley Hill, Adam Gleave, Anssi Kanervisto, Maximilian Ernestus, and Noah Dormann. Stable-baselines3: Reliable reinforcement learning implementations. *Journal of Machine Learning Research*, 22(268):1–8, 2021. URL <http://jmlr.org/papers/v22/20-1364.html>.
- Olivier Roy and Martin Vetterli. The effective rank: A measure of effective dimensionality. In *2007 15th European Signal Processing Conference*, pp. 606–610, 2007.
- John Schulman, Sergey Levine, Pieter Abbeel, Michael Jordan, and Philipp Moritz. Trust region policy optimization. In Francis Bach and David Blei (eds.), *Proceedings of the 32nd International Conference on Machine Learning*, volume 37 of *Proceedings of Machine Learning Research*, pp. 1889–1897, Lille, France, 07–09 Jul 2015a. PMLR. URL <https://proceedings.mlr.press/v37/schulman15.html>.
- John Schulman, Philipp Moritz, Sergey Levine, Michael Jordan, and Pieter Abbeel. High-dimensional continuous control using generalized advantage estimation. *arXiv preprint arXiv:1506.02438*, 2015b.
- John Schulman, Filip Wolski, Prafulla Dhariwal, Alec Radford, and Oleg Klimov. Proximal policy optimization algorithms. *arXiv preprint arXiv:1707.06347*, 2017.
- C. Spearman. The proof and measurement of association between two things. *The American Journal of Psychology*, 100(3/4):441–471, 1987. ISSN 00029556. URL <http://www.jstor.org/stable/1422689>.

- Mingfei Sun, Vitaly Kurin, Guoqing Liu, Sam Devlin, Tao Qin, Katja Hofmann, and Shimon Whiteson. You may not need ratio clipping in ppo. *arXiv preprint arXiv:2202.00079*, 2022.
- Richard S Sutton and Andrew G Barto. *Reinforcement learning: An introduction*. MIT press, 2018.
- Richard S Sutton, David McAllester, Satinder Singh, and Yishay Mansour. Policy gradient methods for reinforcement learning with function approximation. In S. Solla, T. Leen, and K. Müller (eds.), *Advances in Neural Information Processing Systems*, volume 12. MIT Press, 1999. URL https://proceedings.neurips.cc/paper_files/paper/1999/file/464d828b85b0bed98e80ade0a5c43b0f-Paper.pdf.
- Csaba Szepesvári. *Algorithms for reinforcement learning*. Springer Nature, 2022.
- Emanuel Todorov, Tom Erez, and Yuval Tassa. Mujoco: A physics engine for model-based control. In *2012 IEEE/RSJ International Conference on Intelligent Robots and Systems*, pp. 5026–5033. IEEE, 2012. doi: 10.1109/IROS.2012.6386109.
- Mark Towers, Jordan K. Terry, Ariel Kwiatkowski, John U. Balis, Gianluca de Cola, Tristan Deleu, Manuel Goulão, Andreas Kallinteris, Arjun KG, Markus Krimmel, Rodrigo Perez-Vicente, Andrea Pierré, Sander Schulhoff, Jun Jet Tai, Andrew Tan Jin Shen, and Omar G. Younis. Gymnasium, March 2023. URL <https://zenodo.org/record/8127025>.
- Yuhui Wang, Hao He, and Xiaoyang Tan. Truly proximal policy optimization. In Ryan P. Adams and Vibhav Gogate (eds.), *Proceedings of The 35th Uncertainty in Artificial Intelligence Conference*, volume 115 of *Proceedings of Machine Learning Research*, pp. 113–122. PMLR, 22–25 Jul 2020. URL <https://proceedings.mlr.press/v115/wang20b.html>.
- Yuzhe Yang, Guo Zhang, Zhi Xu, and Dina Katabi. Harnessing structures for value-based planning and reinforcement learning. In *International Conference on Learning Representations*, 2020. URL <https://openreview.net/forum?id=rklHqRVKvH>.

A Additional background

A.1 Reinforcement Learning

The undiscounted formulation presented in the background (Section 2) has also been used by Schulman et al. (2015b) and does not limit the use of a discount factor to discount future rewards; for that purpose, as we consider a finite-horizon setting, we can assume that discounting would already be present in the reward which depends on time through the state. This allows to isolate the discount factor γ for the purpose of the value estimation with GAE which serves as a trade-off between the bias and the variance in the estimator, in addition to λ used for the λ -returns that combine multiple n -step returns. More importantly, this also allows us to reuse the policy gradient and PPO losses without discount factors, as the deep RL community is used to them while avoiding their incorrect use in the discounted setting as pointed out by Nota & Thomas (2020). In any case, our results can also be translated to the discounted setting using a biased gradient estimator (missing a discount factor), being the typical setting considered in deep RL works.

B Experiment details

B.1 Code and run histories

Our codebase is publicly available at <https://github.com/CLAIRE-Labo/no-representation-no-trust>. It includes the development environment distributed as a Docker image for GPU-accelerated machines and a Conda environment for MPS-accelerated machines, the training code, scripts to run all the experiments, and the notebook that generated the plots. The codebase uses TorchRL (Bou et al., 2024) and provides a comprehensive toolbox to study representation dynamics in policy optimization. We also provide modified scripts of CleanRL (Huang et al., 2022b) to replicate the collapse observed in this work and ensure it is not a bug from our novel codebase.

The code repository contains links to the Weights&Biases (W&B) project with all of our run histories, a summary W&B report of the runs, and a W&B report with the replication with CleanRL.

Runs are fully reproducible on the same acceleration device on which they were run. In particular, we have reproduced our results on three different clusters with the same NVIDIA GPU device.

B.2 Additional details on our experimental setup

We conduct experiments on an environment with pixel-based observations and discrete actions and an environment with continuous observations and actions, each with a different model architecture. For the discrete action case, we use the Arcade Learning Environment (ALE)(Bellemare et al., 2013) with the specification recommended by Machado et al. (2018) in v5 on Gymnasium (Towers et al., 2023). That is, with a sticky action probability of 0.25 as the only form of environment stochasticity, using only the game-over signal for termination (as opposed to end-of-life signals) with the default maximum of 108×10^3 environment frames per episode and reporting performance over training episodes (i.e., with sampling according to the policy distribution as opposed to taking the mode action). We train all models for 100 million environment frames. We use standard algorithmic choices to make our setting and results relevant to previous work. This includes taking only the sign of rewards (clipping) and frame skipping. We use a frame skip of 3, as opposed to the standard value of 4, due to limitations in the ALE-v5 environment, which does not implement frame pooling.⁵ We use the standard architecture of Mnih et al. (2015) consisting of convolutional layers followed by linear layers, all with ReLU activations, and no normalization layers. We also use Mnih et al. (2015)’s standard observation transformations with a resizing to 84x84, grayscaling, and a frame stacking of 4.

For the continuous case, we use MuJoCo (Todorov et al., 2012) with v4 on Gymnasium (Towers et al., 2023) with the default maximum of 1,000 environment frames to mark episode termination. Similarly to Atari, we report performance as the average episode return over training episodes. We

⁵That is taking the max over the last two skipped and unskipped frames to capture elements that only appear in even or odd frames of the game (<https://github.com/Farama-Foundation/Arcade-Learning-Environment/issues/467>). Using an odd frame skip value alleviates the issue.

train all models for 5 million environment frames. We standardize the observations (subtract mean and divide by standard deviation) according to an initial rollout of 4,000 environment steps (at least four episodes). The standardization parameters are kept the same to avoid adding non-stationarity. We use the same architecture as Schulman et al. (2017), with only linear layers, tanh activations, and no normalization layers. We also experiment with ReLU activations. The network outputs a mean and a standard deviation (with softplus), both conditioning on the observation independently for each action dimension, which are then used to create a TanhNormal distribution, similarly to Haarnoja et al. (2018).

To measure the plasticity loss of a checkpoint, we use the same optimization hyperparameters used to train the checkpoint, i.e. the same batch size and learning rate. The dataset sizes and fitting budgets for plasticity are listed in Tables 2 and 3.

We provide a high-level pseudocode for PPO in Algorithm 1 and list all hyperparameters considered in Tables 2 and 3.

Algorithm 1 High-level Pseudocode for PPO

N : number of environments in parallel.
 B_{env} : agent steps per environment to collect in a batch.
 K : number of optimization epochs per batch.

$L_{\pi_{\text{old}}}^{\text{CLIP}}(\boldsymbol{\theta})$: PPO-Clip objective.
 $H(\boldsymbol{\theta})$: entropy bonus/loss; c_H : entropy bonus coefficient.
 $L^{VF}(\mathbf{w})$: critic loss (L^2 to GAE); c_{VF} : critic loss coefficient.

- 1: **while** collected environment steps \leq total environment steps **do**
 Collect a batch of interaction steps of size $B = N \times B_{\text{env}}$ and computes advantages.
- 2: **for** actor = 1 **to** N **do**
- 3: Run policy π_{old} in environment for B_{env} agent steps.
- 4: Compute advantage estimates $\Psi_1^{\text{actor}}, \dots, \Psi_{B_{\text{env}}}^{\text{actor}}$ with GAE.
- 5: **end for**
- 6: Minimize overall policy and value loss ($-L_{\pi_{\text{old}}}^{\text{CLIP}}(\boldsymbol{\theta}) - c_H H(\boldsymbol{\theta}) + c_{VF} L^{VF}(\mathbf{w})$) with autograd on the on the collected batch over K epochs with minibatch size $M \leq B$.
- 7: $\pi_{\text{old}} \leftarrow \pi_{\boldsymbol{\theta}}$
- 8: **end while**

Proximal Feature Regularization With a coefficient c_{PFO} , the PFO loss is added to the overall loss ($-L_{\pi_{\text{old}}}^{\text{CLIP}}(\boldsymbol{\theta}) + c_{PFO} L_{\pi_{\text{old}}}^{\text{PFO}}(\boldsymbol{\theta}) - c_H H(\boldsymbol{\theta}) + c_{VF} L^{VF}(\mathbf{w})$) optimized with autograd over multiple minibatch epochs.

Table 1: Hyperparameters for the toy setting in Figure 5.

Environment	
$\phi(x)$	Sampled from a Normal distribution
$\phi(y)$	$\alpha\phi(x)$
α	3 (overshoot), -1 (interfere)
$A(x, a_1), A(y, a_1)$	1
Policy	
Network	2 output neurons representing the 2 logits + Softmax
Optimization	
Clipping epsilon (PPO-Clip)	0.1
Optimizer	SGD
Learning rate	1.5
Minibatch size	1
Number of epochs	10
Number of steps	20 alternating between x and y

B.3 Additional details on metrics used in the figures

Training curves A point in the training curves in Figures 1, 2, 3, before aggregating seeds and smoothing, corresponds to an average value over the last batch collected at the time of logging for metrics available at every batch (feature rank, entropy, etc.) or the latest batch where the metric was available at the time of logging for the episodic return (as it’s only available when episodes finish, and it requires multiple batches to finish an episode). E.g., in Figure 1 on ALE, a feature rank corresponds to the average feature rank over all the states in the last batch collected at the time of logging and is logged every 0.1% of the batches (i.e. every 6,144 env steps); A return corresponds to the average return across all workers that had episodes finished in the latest batch containing finished episodes at the time of logging.

Figure 4 A window of size 1% of training progress represents approximately 1 million training steps on ALE and 50,000 training steps on MuJoCo We average the metrics per window and then take the 20 windows with the lowest average probability ratios below $1 - \epsilon$. The probability ratios in a run can be trivially within the $1 - \epsilon$ region after the model collapses, resulting in less than 20 points if the model collapses before 20% of the training progress. When all runs give 20 points, we can observe 300 points in total per scatter plot.

Figure 6 A window of size 5% of training progress represents approximately five million training steps in ALE and captures at least five episodes per environment so in total at least 40 episodes. For MuJoCo this represents approximately 256,000 training steps and captures at least 128 episodes per environment so in total at least 256 episodes.

When a model collapses, it typically doesn’t change anymore so its optimization trivially gives ratios within the clipping limits (no value above $1 + \epsilon$ and below $1 - \epsilon$ is logged). In that case, we are more interested in the evolution of the excess ratio before the ratios become trivial. Therefore, the upper limit of the 5% of training progress is taken such that it is the latest timestep where there are at least 10 non-trivial ratios, i.e. 10 logged excess ratios. This coincides with a window before the collapse of the model capturing the values we are interested in. Note that when a model collapses this window may not coincide with the window used to report the other metrics such as the average return, however, these other metrics typically do not change after a collapse, so it is more robust to capture them at the end of training rather than looking for an arbitrary window after the collapse. We give training curves similar to Figure 1 with the interventions performed.

In MuJoCo, with continuous action distributions the ratios diverge to infinity and 0 before collapse therefore to get meaningful plots, we clip average probability ratios above $1 + \epsilon$ and below $1 - \epsilon$ to 10^{12} and 10^{-12} , respectively, before computing the average excess ratio.

We group the different epoch configurations of an intervention on the same environment, giving 15 runs per boxplot (three epochs with five seeds each).

B.4 Statistical significance

Stochasticity in our experiments arises from network initialization, environment transitions (e.g., sticky actions in ALE), agent action sampling, and minibatch sampling for optimization. A seed fully controls the sequence of randomness in a run with the same hyperparameter configuration. We repeat each configuration with five seeds using the same collection of seeds, resulting in the same initialization of the networks and environments for a given seed across configurations. This form of repeated measures allows us to compare the configurations with lower variance as they share the same initial conditions, hence requiring a lower number of seeds.

In Figures 1 and 2, we aggregate the five runs of each experiment into mean curves with min/max shaded areas. The use of min/max error bars allows us to demonstrate the full range of observed outcomes, although it may result in shaded areas that overlap more than with other types of error bars. Most of the claims we make based on those figures do not rely on non-overlapping shaded areas and are instead stronger when the max or min boundaries are consistent with the observation made (min boundary of feature norm increasing, max boundary of feature rank decreasing). Otherwise, we made comparative claims when shaded areas did not overlap (feature rank decreasing faster with more epochs and more non-stationarity).

Figure 3 displays individual seeds to zoom on single-run dynamics around collapse. It is used for an illustrative purpose to provide intuition and does not depend on the number of runs or statistical

aggregation of results. The main claim made with the intuition (breakdown of the trust region) is backed by Figure 4, which includes 300 points per plot per environment, subsampled from 15 training curves per environment.

To evaluate the effects of the interventions in Figure 6, we show boxplots to give a complete idea of the distribution of the data which is formed by grouping the different configurations in the same environment. Each boxplot contains 15 runs. We make claims such as preventing collapse using the tails and medians and claims about lower excess ratio and higher rank using the interquartile range. Without a clear intuition about the distribution of combined configurations per environment, we consider this approach appropriate for comparing interventions.

In summary, we believe our experimental design provides a balanced tradeoff between statistical significance and richness of claims. The computational cost of running more seeds may not yield proportionately valuable insights.

B.5 Hardware and runtime

The experiments in this project took a total of ~11,300 GPU hours on NVIDIA V100 and A100 GPUs (ALE) and ~25,500 CPU hours (MuJoCo). A run on ALE takes around 10 hours on an A100 and 16 hours on a V100. A run on MuJoCo takes around 5 hours on 6 CPUs.

Table 2: Hyperparameters for ALE.

Environment	
Repeat action probability (Sticky actions)	0.25
Frameskip	3
Max environment steps per episode	108,000
Noop reset steps	0
Observation transforms	
Grayscale	True
Resize width ('resize_w')	84
Resize height ('resize_h')	84
Frame stack	4
Normalize observations	False
Reward transforms	
Sign	True
Collector	
Total environment steps	100,000,000
Num envs in parallel	8
Num envs in parallel plasticity	1
Agent steps per batch	10,24 (128 per env)
Total agent steps plasticity	36,000 (at least one full episode)
Models (actor and critic)	
Activation	ReLU
Convolutional Layers	
Filters	[32, 64, 64]
Kernel sizes	[8, 4, 3]
Strides	[4, 2, 1]
Linear Layers	
Number of layers	1
Layer size	512
Optimization	
Advantage estimator	
Advantage estimator	GAE
Gamma	0.99
Lambda	0.95
Value loss	
Value loss coefficient	0.5
Loss type	L2
Policy loss	
Normalize advantages	minibatch normalization
Clipping epsilon	0.1
Entropy coefficient	0.01
Feature regularization coefficient	1 (last pre-activation), 10 (all pre-activations)
Optimizer (actor and critic)	
Optimizer	Adam
Learning rate	0.00025
Betas	(0.9, 0.999), (0.9, 0.9) for the intervention
Max grad norm	0.5
Annealing linearly	False
Number of epochs	4, 6, 8
Number of epochs plasticity fit	1
Minibatch size	256
Logging (% of the total number of batches)	
Training	every 0.1% (~100,000 env steps)
Plasticity	every 2.5% (41 times in total)

Table 3: Hyperparameters for MuJoCo.

Environment	
Frameskip	1
Max env steps per episode	1,000
Noop reset steps	0
Observation transforms	
Normalize observations	True (from initial steps collected by uniform policy)
Initial random steps for normalization	4000 (at least 4 episodes)
Collector	
Total environment steps	5,000,000
Num envs in parallel	2
Num envs in parallel plasticity	4
Agent steps per batch	2048 (1024 per env)
Total environment steps plasticity	4,000 (at least 4 full episodes)
Models (actor and critic)	
Activation	Tanh, ReLU
Convolutional layers	
Number of Layers	0
Linear layers	
Number of layers	2
Layer size	64
Optimization	
Advantage estimator	
Advantage estimator	GAE
Gamma	0.99
Lambda	0.95
Value loss	
Value coefficient	0.5
Loss type	L2
Policy loss	
Normalize advantages	minibatch normalization
Clipping epsilon (PPO-Clip)	0.2
Entropy coefficient	0.0
Feature regularization coefficient	1 (tanh), 10 (ReLU)
Optimizer (actor and critic)	
Optimizer	Adam
Learning rate	0.0003
Betas	(0.9, 0.999), (0.9, 0.9) for the intervention
Max grad norm	0.5
Annealing linearly	False
Number of epochs	10, 15, 20
Number of epochs plasticity fit	4
Minibatch size	64
Logging (% of the total number of batches)	
Training	every 0.1% (6,144 env steps)
Plasticity	every 2.5% (41 times in total)

C Toy setting derivation details

The derivatives of the softmax probability $\pi_{\theta}(a_1|s)$ with respect to θ_1 and θ_2 are as follows:

$$\frac{\partial \pi_{\theta}(a_1|s)}{\partial \theta_1} = \frac{\partial}{\partial \theta_1} \left(\frac{e^{\theta_1 \phi(s)}}{e^{\theta_1 \phi(s)} + e^{\theta_2 \phi(s)}} \right) = \phi(s) \cdot \frac{e^{\theta_1 \phi(s)} \cdot e^{\theta_2 \phi(s)}}{(e^{\theta_1 \phi(s)} + e^{\theta_2 \phi(s)})^2} \quad (3)$$

$$\frac{\partial \pi_{\theta}(a_1|s)}{\partial \theta_2} = \frac{\partial}{\partial \theta_2} \left(\frac{e^{\theta_1 \phi(s)}}{e^{\theta_1 \phi(s)} + e^{\theta_2 \phi(s)}} \right) = -\phi(s) \cdot \frac{e^{\theta_1 \phi(s)} \cdot e^{\theta_2 \phi(s)}}{(e^{\theta_1 \phi(s)} + e^{\theta_2 \phi(s)})^2} \quad (4)$$

The update rule for each parameter θ_i in θ with SGD is $\theta_i^{\text{new}} = \theta_i + \eta \frac{\partial L}{\partial \theta_i}$ where η is the learning rate. Therefore, given the partial derivatives, the updated values for θ_1 and θ_2 after taking a gradient step are (if the probability is still inferior to $1 + \epsilon$, otherwise the gradient is 0)

$$\theta_1^{\text{new}} = \theta_1 + \eta \cdot \frac{A(s, a_1)}{\pi_{\text{old}}(a_i|s)} \cdot \left(\phi(s) \cdot \frac{e^{\theta_1 \phi(s)} \cdot e^{\theta_2 \phi(s)}}{(e^{\theta_1 \phi(s)} + e^{\theta_2 \phi(s)})^2} \right) \quad \text{and} \quad \theta_2^{\text{new}} = \theta_2 - \eta \cdot \frac{A(s, a_1)}{\pi_{\text{old}}(a_i|s)} \cdot \left(\phi(s) \cdot \frac{e^{\theta_1 \phi(s)} \cdot e^{\theta_2 \phi(s)}}{(e^{\theta_1 \phi(s)} + e^{\theta_2 \phi(s)})^2} \right)$$

Hence,

$$\begin{aligned} \theta_1^{\text{new}} &= \theta_1 + \delta_s \quad \text{with} \quad \delta_s = \eta \cdot \frac{A(s, a_1)}{\pi_{\text{old}}(a_i|s)} \cdot \left(\phi(s) \cdot \frac{e^{\theta_1 \phi(s)} \cdot e^{\theta_2 \phi(s)}}{(e^{\theta_1 \phi(s)} + e^{\theta_2 \phi(s)})^2} \right) \\ \theta_2^{\text{new}} &= \theta_2 - \delta_s \end{aligned}$$

Let $\alpha \geq 0$ and without loss of generality, let's take $\alpha \geq 1$. After a gradient step on x one has

$$\begin{aligned} \pi_{\theta^{\text{new}}}(a_1|x) &= \frac{e^{\theta_1^{\text{new}} \phi(x)}}{e^{\theta_1^{\text{new}} \phi(x)} + e^{\theta_2^{\text{new}} \phi(x)}} \\ &= \frac{e^{(\theta_1 + \delta_x) \phi(x)}}{e^{(\theta_1 + \delta_x) \phi(x)} + e^{(\theta_2 - \delta_x) \phi(x)}} \\ &= \frac{e^{\theta_1 \phi(x)}}{e^{\theta_1 \phi(x)} + e^{(\theta_2 - 2\delta_x) \phi(x)}} \\ &= \frac{e^{\theta_1 \phi(x)}}{e^{\theta_1 \phi(x)} + e^{\theta_2 \phi(x) - 2\delta_x \phi(x)}} \\ &\geq \frac{e^{\theta_1 \phi(x)}}{e^{\theta_1 \phi(x)} + e^{\theta_2 \phi(x)}} \quad (\text{since } -2\delta_x \phi(x) \leq 0) \\ &= \pi_{\theta}(a_1|x) \end{aligned}$$

$$\begin{aligned} \pi_{\theta^{\text{new}}}(a_1|y) &= \frac{e^{\theta_1^{\text{new}} \alpha \phi(x)}}{e^{\theta_1^{\text{new}} \alpha \phi(x)} + e^{\theta_2^{\text{new}} \alpha \phi(x)}} \\ &= \frac{e^{(\theta_1 + \delta_x) \alpha \phi(x)}}{e^{(\theta_1 + \delta_x) \alpha \phi(x)} + e^{(\theta_2 - \delta_x) \alpha \phi(x)}} \\ &= \frac{e^{\theta_1 \alpha \phi(x)}}{e^{\theta_1 \alpha \phi(x)} + e^{(\theta_2 - 2\delta_x) \alpha \phi(x)}} \\ &= \frac{e^{\theta_1 \alpha \phi(x)}}{e^{\theta_1 \alpha \phi(x)} + e^{\theta_2 \alpha \phi(x) - 2\delta_x \alpha \phi(x)}} \\ &\geq \frac{e^{\theta_1 \alpha \phi(x)}}{e^{\theta_1 \alpha \phi(x)} + e^{\theta_2 \alpha \phi(x)}} \quad (\text{since } -2\delta_x \alpha \phi(x) \leq 0) \\ &= \pi_{\theta}(a_1|y) \end{aligned}$$

And after a gradient step on y :

$$\begin{aligned}
\pi_{\boldsymbol{\theta}^{\text{new}}}(a_1|x) &= \frac{e^{\theta_1^{\text{new}}\phi(x)}}{e^{\theta_1^{\text{new}}\phi(x)} + e^{\theta_2^{\text{new}}\phi(x)}} \\
&= \frac{e^{(\theta_1+\delta_y)\phi(x)}}{e^{(\theta_1+\delta_y)\phi(x)} + e^{(\theta_2-\delta_y)\phi(x)}} \\
&= \frac{e^{\theta_1\phi(x)}}{e^{\theta_1\phi(x)} + e^{(\theta_2-2\delta_y)\phi(x)}} \\
&= \frac{e^{\theta_1\phi(x)}}{e^{\theta_1\phi(x)} + e^{\theta_2\phi(x)-2\delta_y\phi(x)}} \\
&\geq \frac{e^{\theta_1\phi(x)}}{e^{\theta_1\phi(x)} + e^{\theta_2\phi(x)}} \quad (\text{since } -2\delta_y\phi(x) \leq 0) \\
&= \pi_{\boldsymbol{\theta}}(a_1|x)
\end{aligned}$$

$$\begin{aligned}
\pi_{\boldsymbol{\theta}^{\text{new}}}(a_1|y) &= \frac{e^{\theta_1^{\text{new}}\alpha\phi(x)}}{e^{\theta_1^{\text{new}}\alpha\phi(x)} + e^{\theta_2^{\text{new}}\alpha\phi(x)}} \\
&= \frac{e^{(\theta_1+\delta_y)\alpha\phi(x)}}{e^{(\theta_1+\delta_y)\alpha\phi(x)} + e^{(\theta_2-\delta_y)\alpha\phi(x)}} \\
&= \frac{e^{\theta_1\alpha\phi(x)}}{e^{\theta_1\alpha\phi(x)} + e^{(\theta_2-2\delta_y)\alpha\phi(x)}} \\
&= \frac{e^{\theta_1\alpha\phi(x)}}{e^{\theta_1\alpha\phi(x)} + e^{\theta_2\alpha\phi(x)-2\delta_y\alpha\phi(x)}} \\
&\geq \frac{e^{\theta_1\alpha\phi(x)}}{e^{\theta_1\alpha\phi(x)} + e^{\theta_2\alpha\phi(x)}} \quad (\text{since } -2\delta_y\alpha\phi(x) \leq 0) \\
&= \pi(a_1, \alpha x, \boldsymbol{\theta}) \\
&= \pi_{\boldsymbol{\theta}}(a_1|y)
\end{aligned}$$

Let $\alpha \leq 0$ and without loss of generality, let's take $\alpha \leq 1$, after a gradient step on x one has

$$\begin{aligned}
\pi_{\boldsymbol{\theta}^{\text{new}}}(a_1|x) &= \frac{e^{\theta_1^{\text{new}}\phi(x)}}{e^{\theta_1^{\text{new}}\phi(x)} + e^{\theta_2^{\text{new}}\phi(x)}} \\
&= \frac{e^{(\theta_1+\delta_x)\phi(x)}}{e^{(\theta_1+\delta_x)\phi(x)} + e^{(\theta_2-\delta_x)\phi(x)}} \\
&= \frac{e^{\theta_1\phi(x)}}{e^{\theta_1\phi(x)} + e^{(\theta_2-2\delta_x)\phi(x)}} \\
&= \frac{e^{\theta_1\phi(x)}}{e^{\theta_1\phi(x)} + e^{\theta_2\phi(x)-2\delta_x\phi(x)}} \\
&\geq \frac{e^{\theta_1\phi(x)}}{e^{\theta_1\phi(x)} + e^{\theta_2\phi(x)}} \quad (\text{since } -2\delta_x\phi(x) \leq 0) \\
&= \pi_{\boldsymbol{\theta}}(a_1|x)
\end{aligned}$$

$$\begin{aligned}
\pi_{\theta^{\text{new}}}(a_1, y) &= \frac{e^{\theta_1^{\text{new}} \alpha \phi(x)}}{e^{\theta_1^{\text{new}} \alpha \phi(x)} + e^{\theta_2^{\text{new}} \alpha \phi(x)}} \\
&= \frac{e^{(\theta_1 + \delta_x) \alpha \phi(x)}}{e^{(\theta_1 + \delta_x) \alpha \phi(x)} + e^{(\theta_2 - \delta_x) \alpha \phi(x)}} \\
&= \frac{e^{\theta_1 \alpha \phi(x)}}{e^{\theta_1 \alpha \phi(x)} + e^{(\theta_2 - 2\delta_x) \alpha \phi(x)}} \\
&= \frac{e^{\theta_1 \alpha \phi(x)}}{e^{\theta_1 \alpha \phi(x)} + e^{\theta_2 \alpha \phi(x) - 2\delta_x \alpha \phi(x)}} \\
&\leq \frac{e^{\theta_1 \alpha \phi(x)}}{e^{\theta_1 \alpha \phi(x)} + e^{\theta_2 \alpha \phi(x)}} \quad (\text{since } -2\delta_x \alpha \phi(x) \geq 0) \\
&= \pi_{\theta}(a_1 | y)
\end{aligned}$$

And after a gradient step on y :

$$\begin{aligned}
\pi_{\theta^{\text{new}}}(a_1 | x) &= \frac{e^{\theta_1^{\text{new}} \phi(x)}}{e^{\theta_1^{\text{new}} \phi(x)} + e^{\theta_2^{\text{new}} \phi(x)}} \\
&= \frac{e^{(\theta_1 + \delta_y) \phi(x)}}{e^{(\theta_1 + \delta_y) \phi(x)} + e^{(\theta_2 - \delta_y) \phi(x)}} \\
&= \frac{e^{\theta_1 \phi(x)}}{e^{\theta_1 \phi(x)} + e^{(\theta_2 - 2\delta_y) \phi(x)}} \\
&= \frac{e^{\theta_1 \phi(x)}}{e^{\theta_1 \phi(x)} + e^{\theta_2 \phi(x) - 2\delta_y \phi(x)}} \\
&\leq \frac{e^{\theta_1 \phi(x)}}{e^{\theta_1 \phi(x)} + e^{\theta_2 \phi(x)}} \quad (\text{since } -2\delta_y \phi(x) \geq 0) \\
&= \pi_{\theta}(a_1 | x)
\end{aligned}$$

$$\begin{aligned}
\pi_{\theta^{\text{new}}}(a_1 | y) &= \frac{e^{\theta_1^{\text{new}} \alpha \phi(x)}}{e^{\theta_1^{\text{new}} \alpha \phi(x)} + e^{\theta_2^{\text{new}} \alpha \phi(x)}} \\
&= \frac{e^{(\theta_1 + \delta_y) \alpha \phi(x)}}{e^{(\theta_1 + \delta_y) \alpha \phi(x)} + e^{(\theta_2 - \delta_y) \alpha \phi(x)}} \\
&= \frac{e^{\theta_1 \alpha \phi(x)}}{e^{\theta_1 \alpha \phi(x)} + e^{(\theta_2 - 2\delta_y) \alpha \phi(x)}} \\
&= \frac{e^{\theta_1 \alpha \phi(x)}}{e^{\theta_1 \alpha \phi(x)} + e^{\theta_2 \alpha \phi(x) - 2\delta_y \alpha \phi(x)}} \\
&\geq \frac{e^{\theta_1 \alpha \phi(x)}}{e^{\theta_1 \alpha \phi(x)} + e^{\theta_2 \alpha \phi(x)}} \quad (\text{since } -2\delta_y \alpha \phi(x) \leq 0) \\
&= \pi_{\theta}(a_1 | y)
\end{aligned}$$

D Main paper figures on all environments

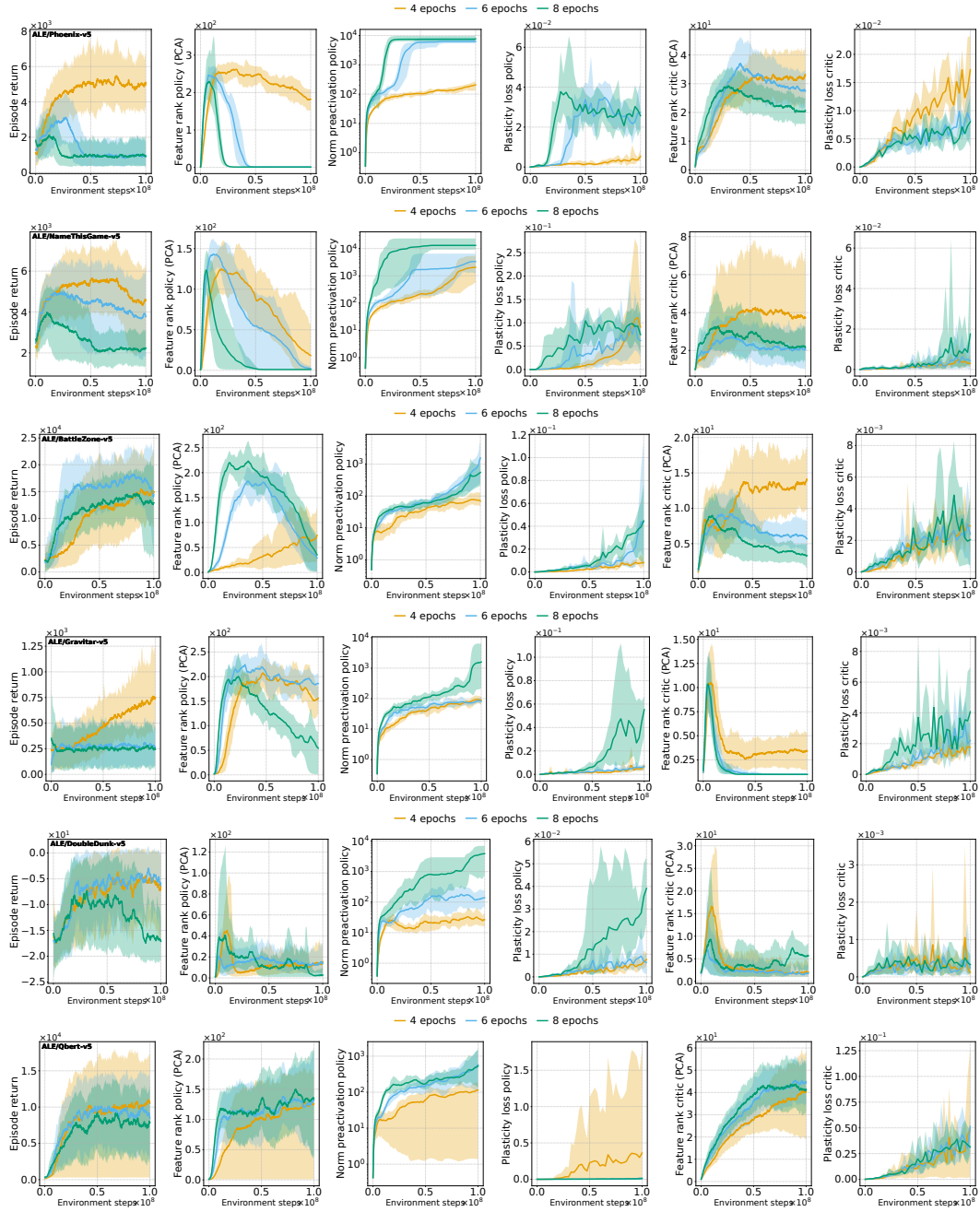


Figure 7: Figure 1 on ALE. Qbert is the only game where rank decline and collapse are not observed, apart from an outlier run that collapsed at initialization. The performance of the policy should be taken into consideration when comparing the plasticity loss of the critic. E.g., for Phoenix, the plasticity loss of the critic associated with the policy the doesn't collapse ends up higher than that of the policies that do collapse.

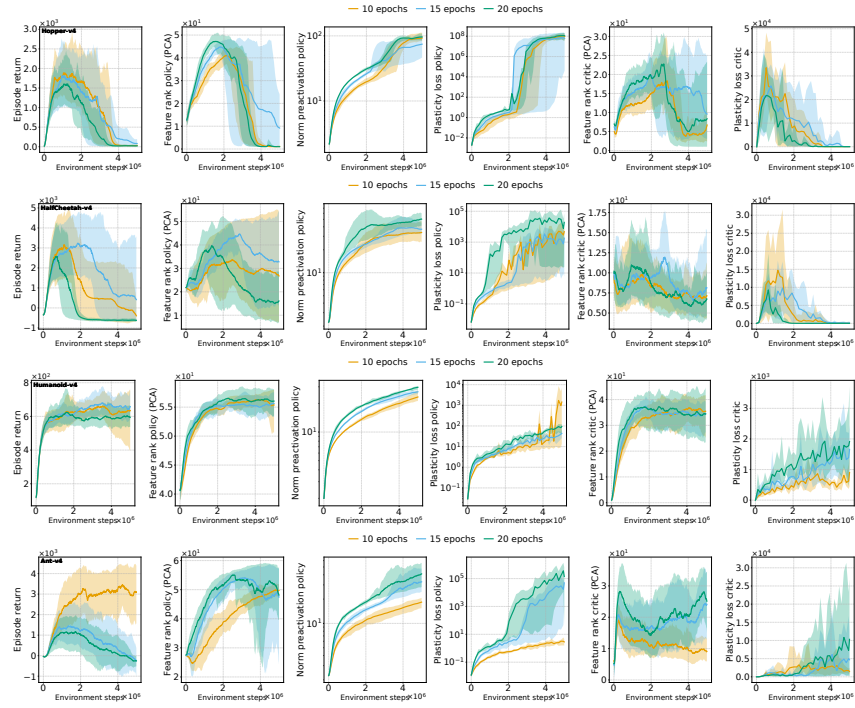


Figure 8: Figure 1 on MuJoCo with the tanh activation.

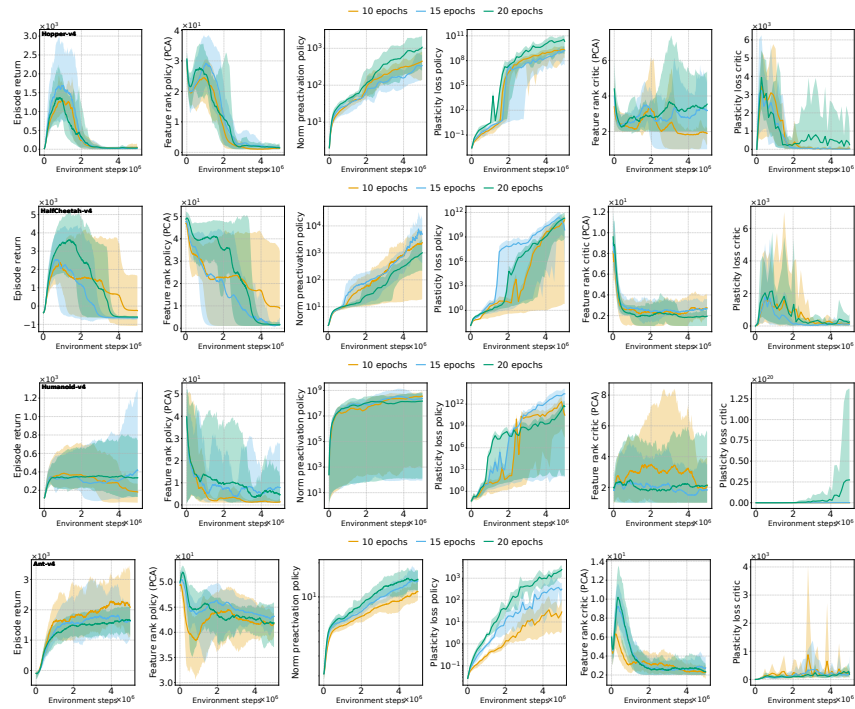


Figure 9: Figure 1 on MuJoCo with the ReLU activation.

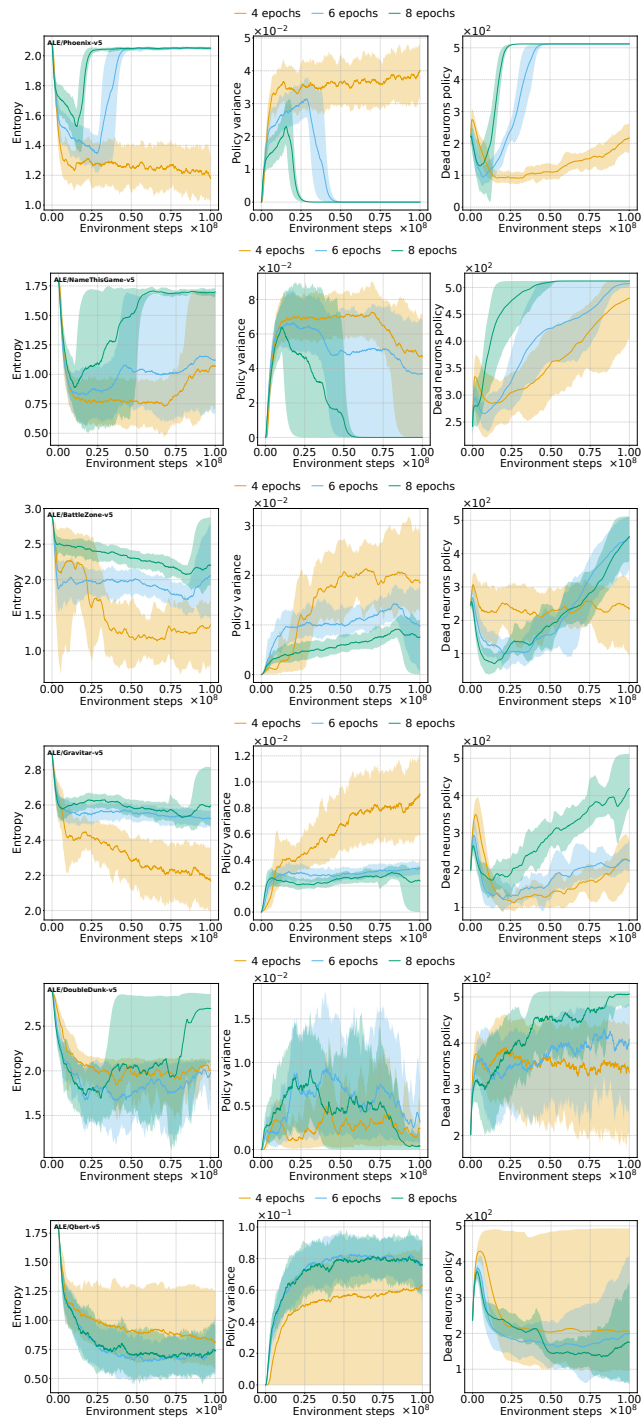


Figure 10: Figure 2 on ALE.

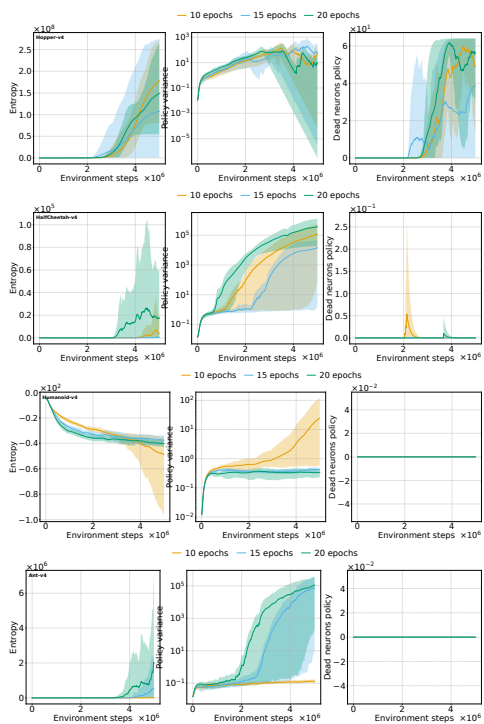


Figure 11: Figure 2 on MuJoCo with the tanh activation. With a continuous action distribution, the policy variance can either drop or explode. Dead neurons for the tanh activation are hard to compute as they are dependent on an arbitrary threshold.

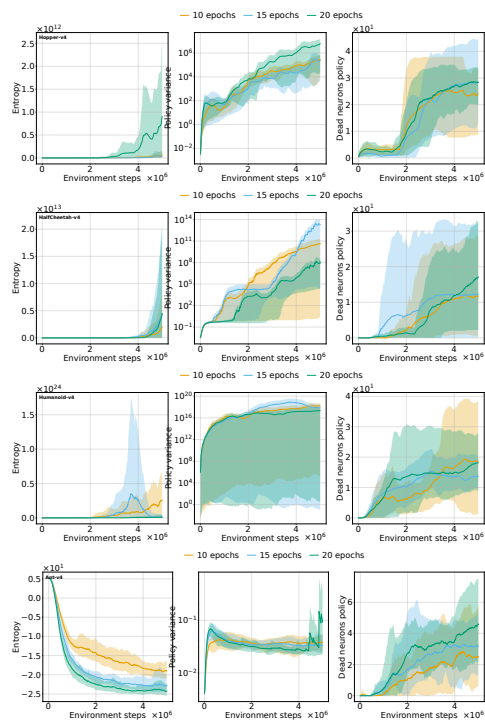


Figure 12: Figure 2 on MuJoCo with the ReLU activation.

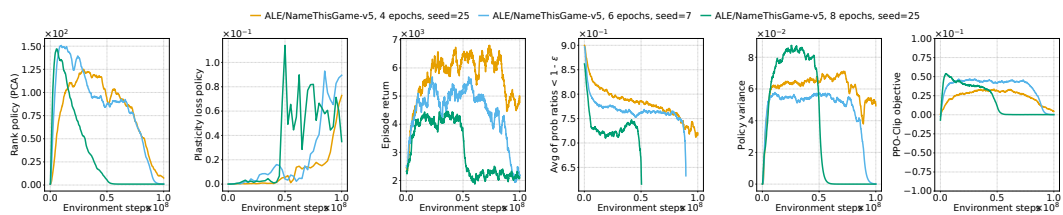


Figure 13: Figure 3 on ALE. (No other environments considered; same figure as Figure 3).

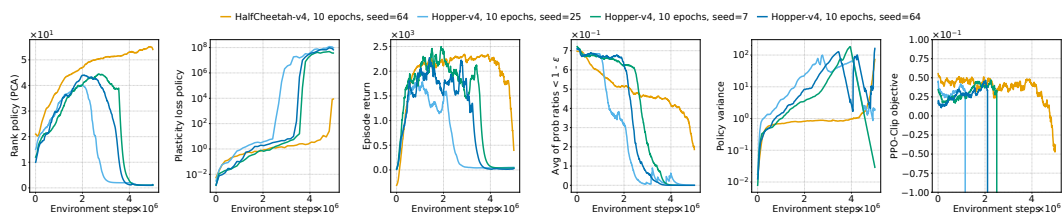


Figure 14: Figure 3 on MuJoCo with the tanh activation. The PPO-Clip objective explodes in the negative direction after collapse so we clip the y-axis of that plot to -1 .

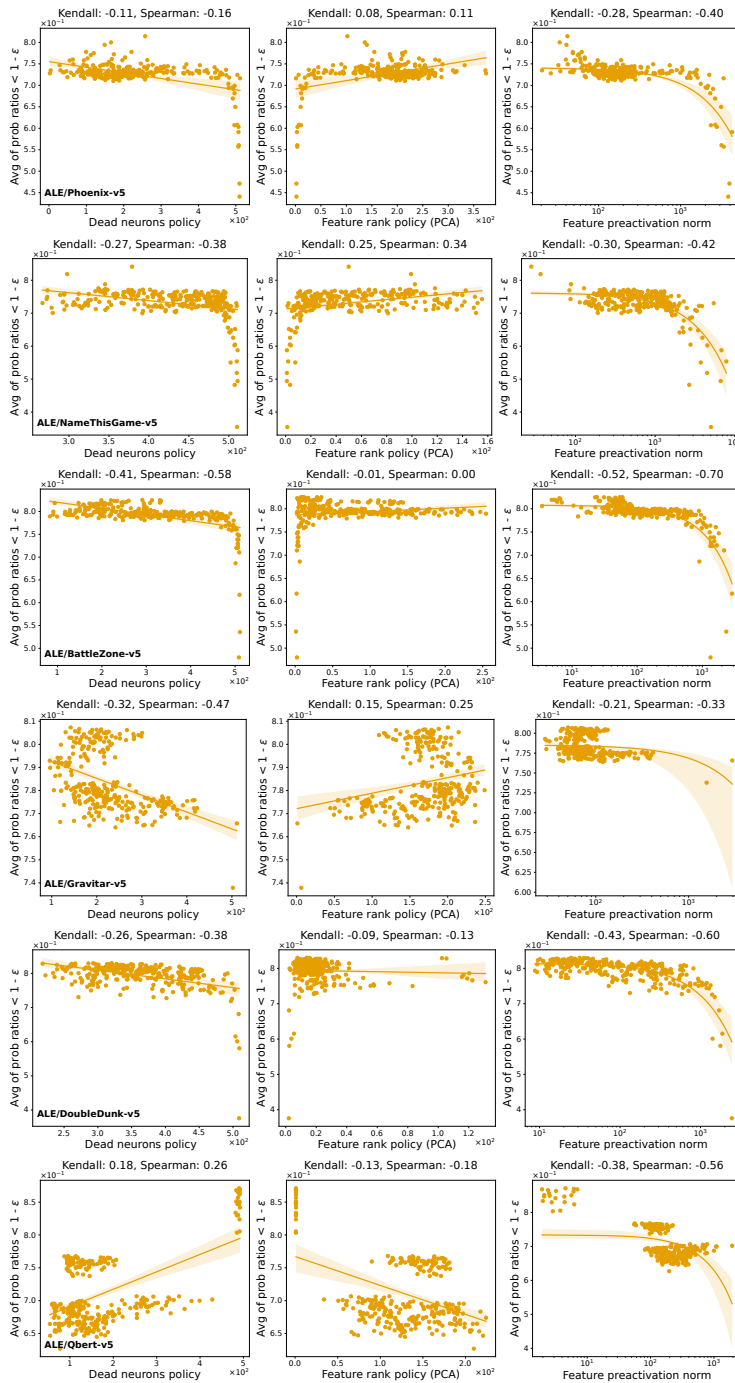


Figure 15: Figure 4 ALE. Qbert and Gravitar do not have runs with poor representation regions (dead neurons > 510) to exhibit the correlation around collapse. Qbert has one outlier where the agent collapsed at the very beginning of the training and kept a high (but lower than 510) number of dead neurons and a trivial rank, but a low excess ratio.

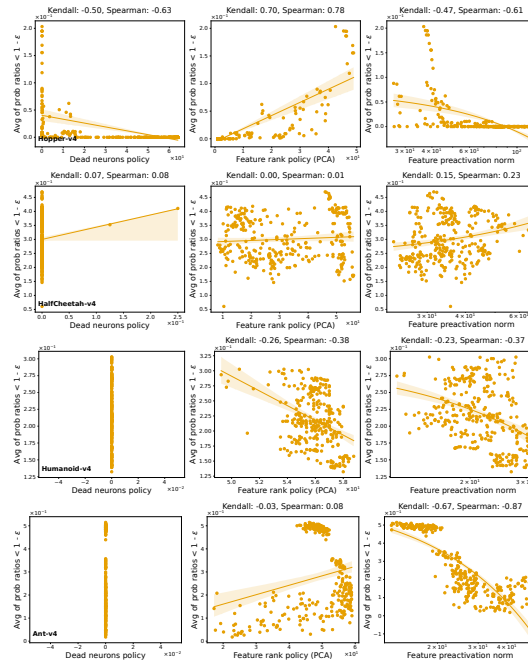


Figure 16: Figure 4 on MuJoCo with the tanh activation. Dead neurons for the tanh activation are hard to compute as they are dependent on an arbitrary threshold. In Humanoid the rank does not arrive at low values to exhibit the correlation around collapse.

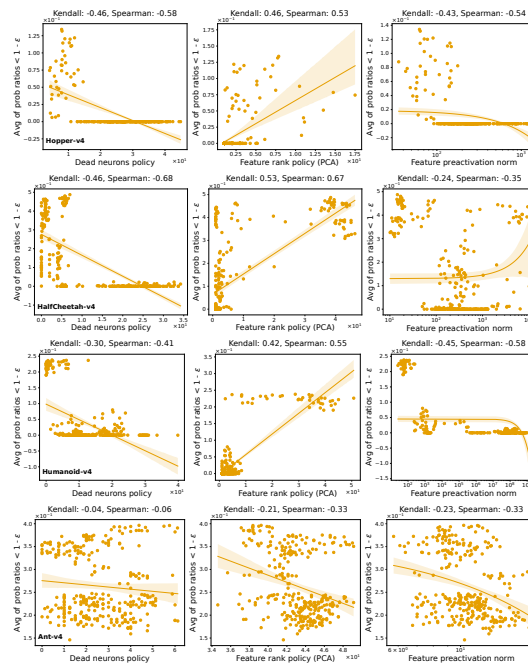


Figure 17: Figure 4 on MuJoCo with the ReLU activation. In Ant, the rank does not arrive at low values to exhibit the correlation around collapse.

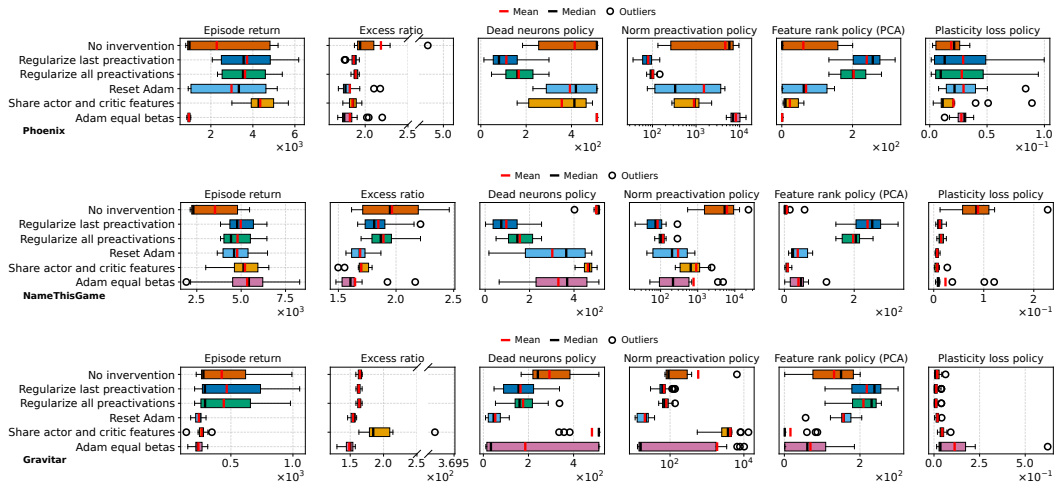


Figure 18: Figure 6 on ALE. The tails of the plasticity loss on Phoenix with interventions can be higher than without interventions on the runs where the models collapse too early without interventions, leading to the plasticity loss of the non-collapsed models with interventions eventually becoming higher. This can be observed from the training curves with interventions. Nevertheless, their medians are lower.

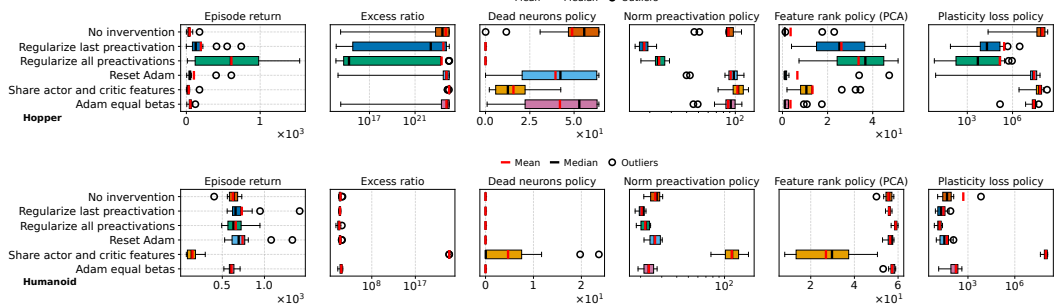


Figure 19: Figure 6 on MuJoCo with the tanh activation.

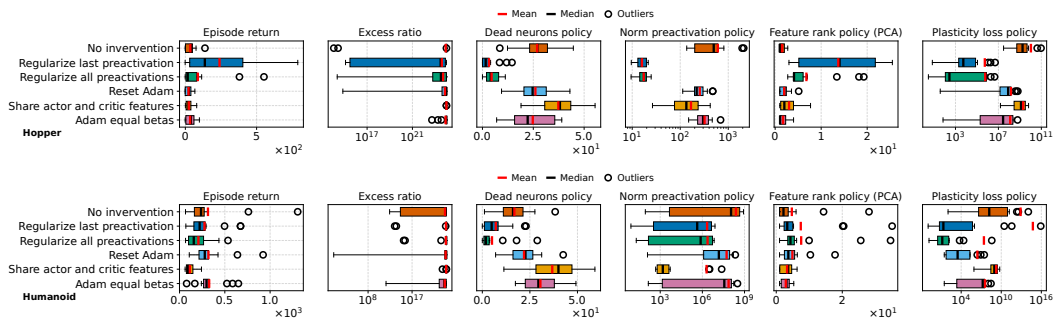


Figure 20: Figure 6 on MuJoCo with the ReLU activation.

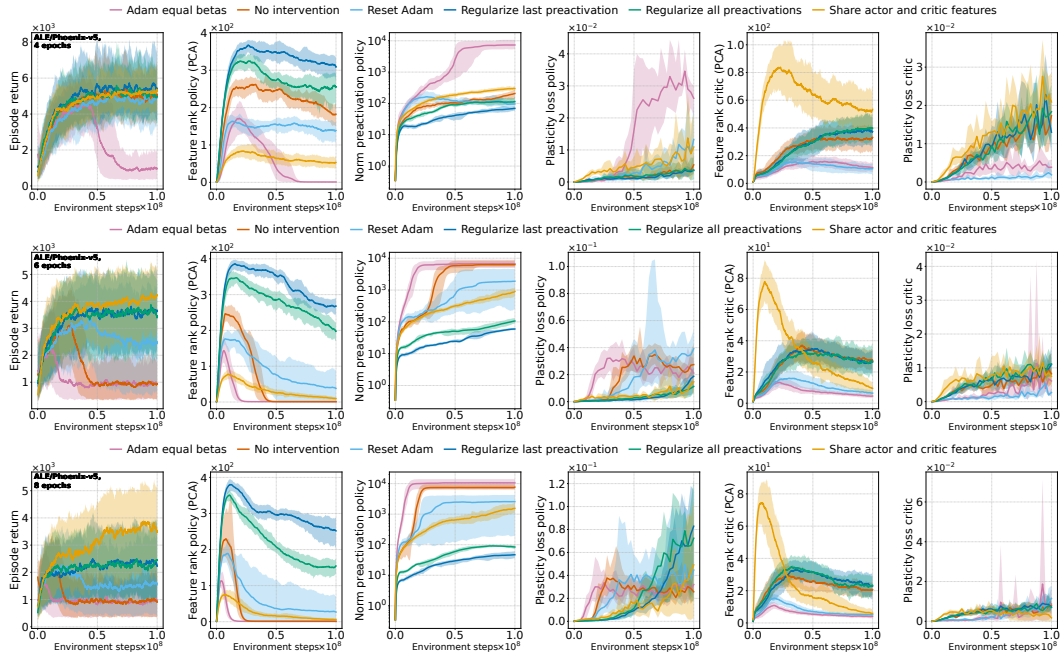


Figure 21: Figure 1 on ALE/Phoenix-v5 with interventions.

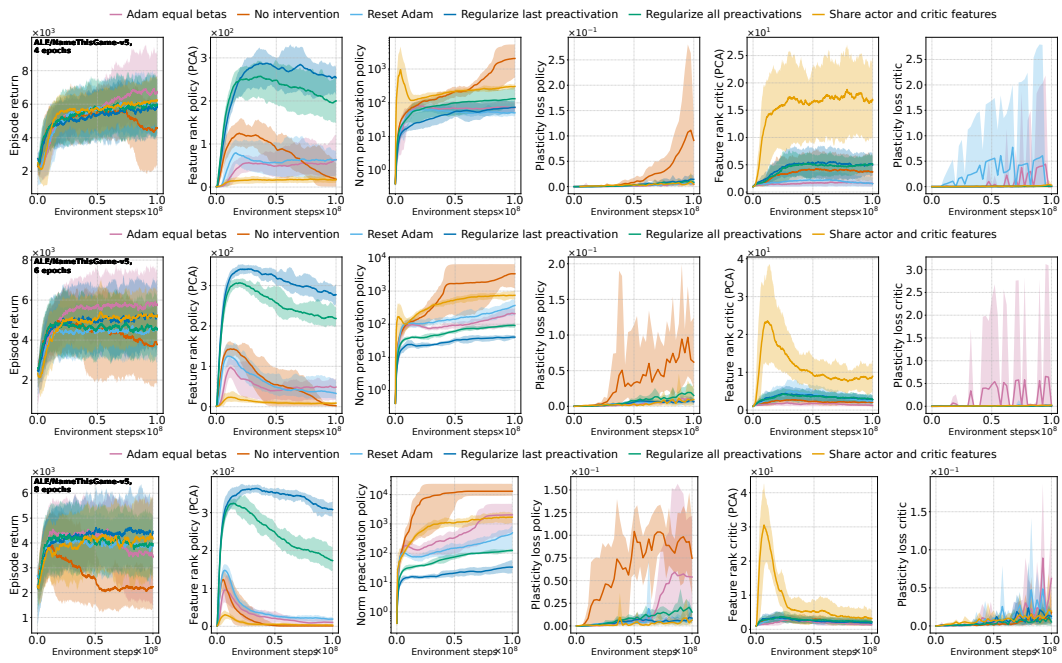


Figure 22: Figure 1 on ALE/NameThisGame-v5 with interventions.

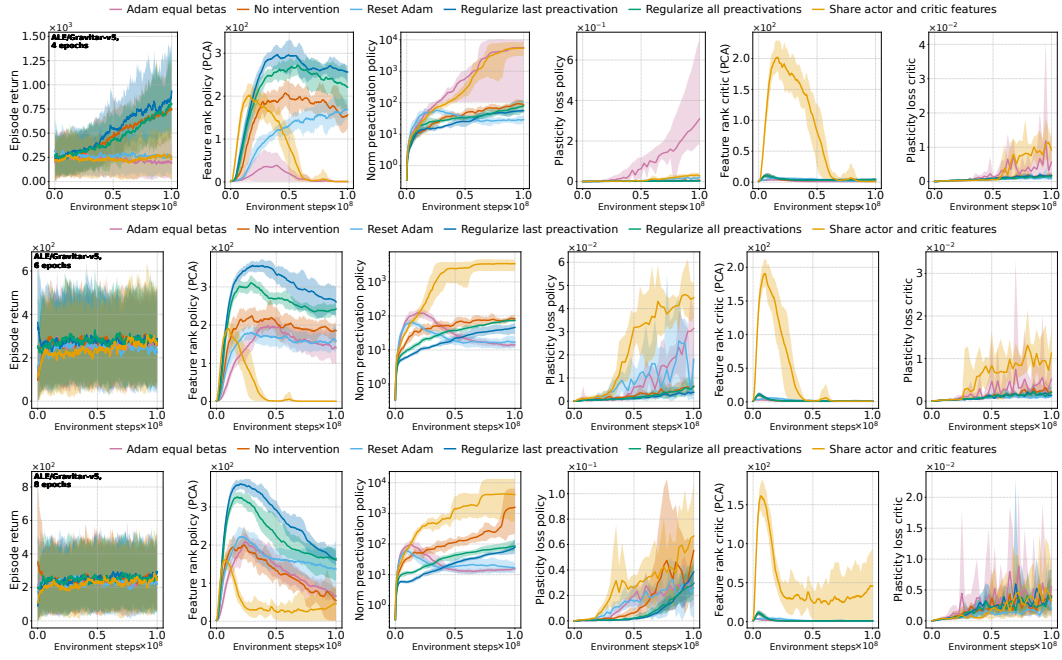


Figure 23: Figure 1 on ALE/NameThisGame-v5 with interventions.

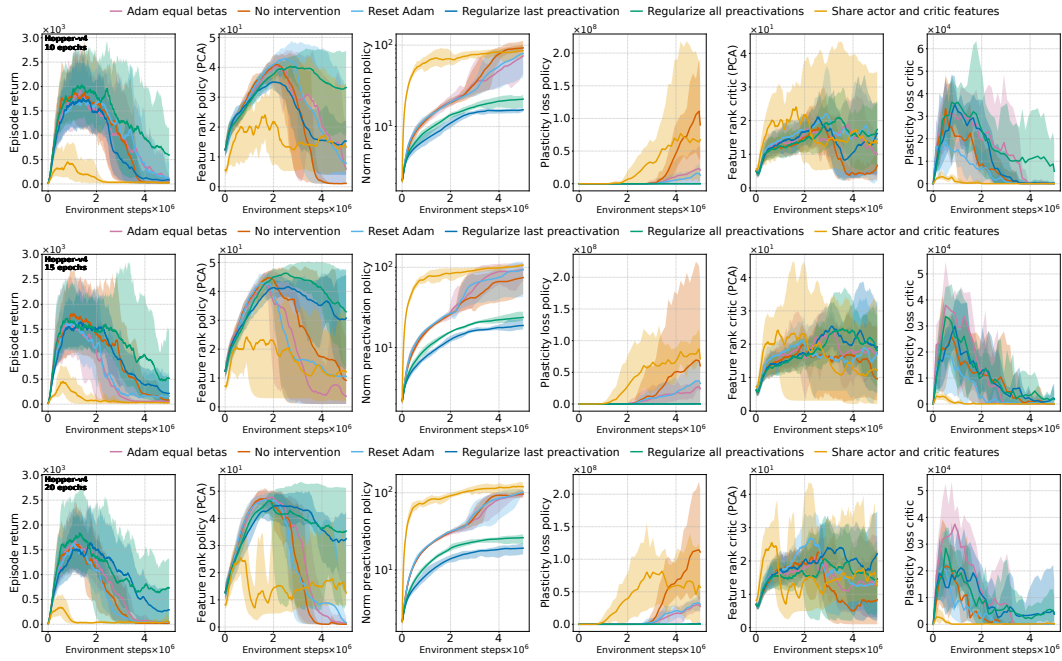


Figure 24: Figure 1 on MuJoCo Hopper with the tanh activation.

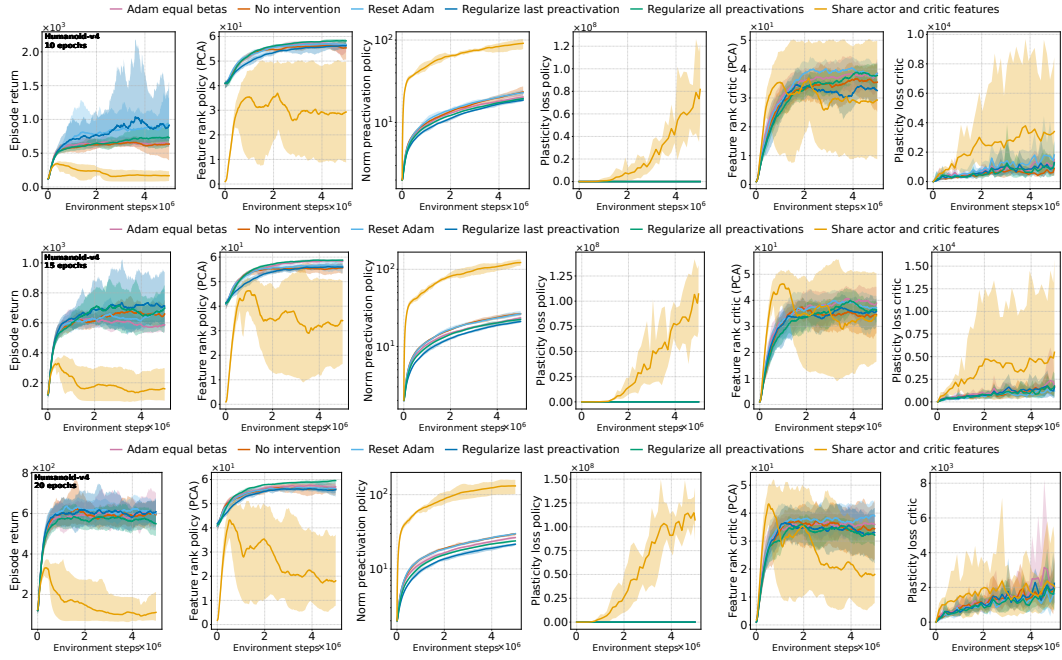


Figure 25: Figure 1 on MuJoCo Humanoid with the tanh activation.

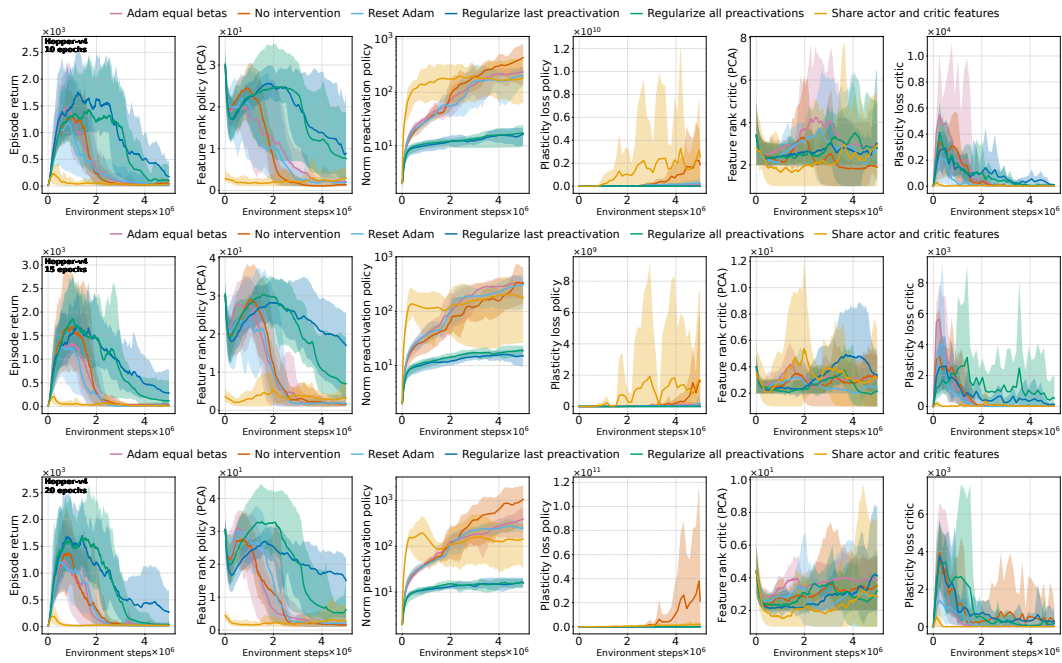


Figure 26: Figure 1 on MuJoCo Hopper with the ReLU activation.

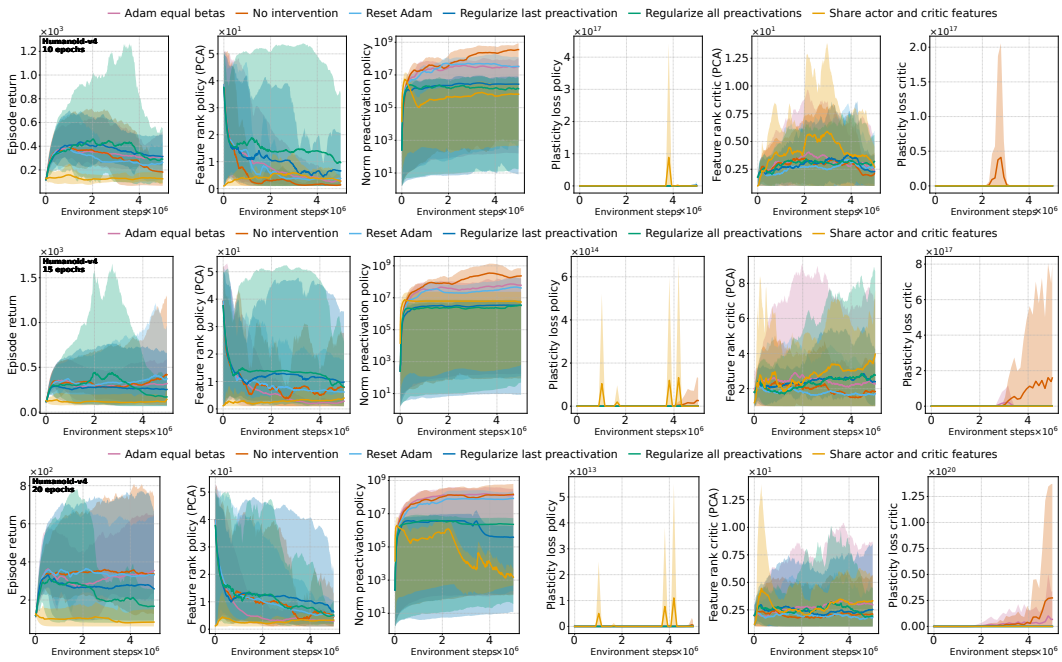


Figure 27: Figure 1 on MuJoCo Humanoid with the ReLU activation.

E Measuring and comparing rank dynamics

Several matrix rank approximations have been used in the deep learning literature, and more specifically the deep RL literature, to measure the rank of the representation of features learned by a deep network. In complement to the background presented in section 2, we give here all the rank metrics we have tracked in this work and their correlations, showing that although their absolute values differ, their dynamics tend to describe the same evolution.

E.1 Definitions of different rank metrics

Essentially, the main difference between the rank metrics considered in the literature is whether they apply a *relative* thresholding of the singular values or an *absolute* one. Their implementation can be found under `src/po_dynamics/modules/metrics.py` in our codebase.

Referring by Φ the $N \times D$ matrix of representations as in Section 2, and letting $\delta = 0.01$ be the threshold, and $\langle \sigma_i(\Phi), \dots, \sigma_D(\Phi) \rangle$ the singular values of Φ in decreasing order, the different rank definitions are as follows.

Effective rank (Roy & Vetterli, 2007) A relative measure of the rank. Let $H(p_1, \dots, p_k)$ denote the Shannon entropy of a probability distribution over k events and $\|\sigma\|_1$ be the sum of the singular values. Let $\tilde{\sigma}_i(\Phi) = \frac{\sigma_i(\Phi)}{\|\sigma\|_1}$ be the normalized singular values. The effective rank is

$$\exp(H(\tilde{\sigma}_1(\Phi), \dots, \tilde{\sigma}_D(\Phi)))$$

This rank measure has also been used in deep learning by Huh et al. (2023).

Approximate rank (PCA) A relative measure of the rank. Intuitively this rank measures the number of PCA values that together explain 99% of the variance of the matrix. This can also be viewed as the lowest-rank reconstruction of the feature matrix with an error lower than 1%.⁶ It is also used in RL by Yang et al. (2020).

$$\min_k \left\{ \frac{\sum_{i=1}^k \sigma_i^2(\Phi)}{\sum_{j=1}^D \sigma_j^2(\Phi)} > 1 - \delta \right\}$$

srank (Kumar et al., 2021) A relative measure of the rank. This is a relative thresholding of the singular values, similar to the approximate rank but with no connection to low-rank reconstruction or variance of the feature matrix.

$$\min_k \left\{ \frac{\sum_{i=1}^k \sigma_i(\Phi)}{\sum_{j=1}^D \sigma_j(\Phi)} > 1 - \delta \right\}$$

Feature Rank (Lyle et al., 2022) An absolute measure of the rank. The number of singular values of the normalized Φ that are larger than a threshold δ .

$$\left| \left\{ \frac{\sigma_i(\Phi)}{\sqrt{N}} > \delta \text{ for } i \in \{1, \dots, D\} \right\} \right|$$

PyTorch rank An absolute measure of the rank. This is the rank computed by `torch.linalg.matrix_rank` and `torch.linalg.matrix_rank`. Let ϵ be the smallest difference possible between points of the data type of the singular values, i.e. for `torch.float32` that is $1.19209e^{-7}$. This rank is computed as follows.

$$\left| \left\{ \frac{\sigma_i(\Phi)}{\sigma_1 \times N} > \epsilon \text{ for } i \in \{1, \dots, D\} \right\} \right|$$

It also appears in Press et al. (2007) in the discussion of SVD solutions for linear least squares.

⁶https://github.com/epfml/ML_course/blob/94d3f8458e31fb619038660ed2704cef3f4bb512/lectures/12/lecture12b_pca_annotated.pdf

E.2 Correlations between the rank metrics

We compute various correlation coefficients and distance measures between the rank metrics. To compute a correlation/distance on a pair of rank metrics (X, Y) , we take for each training run the set $\{(x_t, y_t) | t \in \{0, \dots, T\}\}$ of coinciding values of the curves of the two rank metrics during the run that had T logged steps, compute the correlation/distance on this set, and average the correlation/distance values across all considered runs. We also compute the worst correlation/distance between each rank metric pair for a worst-case analysis. We separate the average values and worst-case values by environment (ALE vs. MuJoCo) for a more granular analysis. We consider all the runs without the interventions and exclude a few runs where the models collapse since the beginning of training, giving constant trivial ranks, as these result in undefined or trivial correlation coefficients.

We compute Kendall's τ coefficient (Kendall, 1938), Spearman's ρ coefficient (Spearman, 1987), the Pearson correlation coefficient, and a normalized L2-distance computed as $\frac{\sqrt{\sum_{t=1}^T (x_t - y_t)^2}}{\sqrt{T} \times L}$ where L is the width of the feature layer considered (i.e., 512 for ALE and 64 for MuJoCo).

Results We visualize the correlation/distance between the pairs of ranks as heatmaps annotated with averages and standard deviations. Overall, the metrics are highly correlated with average correlation coefficients varying between 0.99 and 0.51. Individually, no rank metric correlates significantly more on average with the other metrics. Interestingly, from the average correlations, we clearly see two consistent clusters of stronger correlations between the relative rank metrics (approximate rank (PCA) and Effective rank (Roy & Vetterli, 2007)) and absolute rank metrics (Feature Rank (Lyle et al., 2022) and PyTorch rank). The srnk (Kumar et al., 2021) which is technically a relative metric, but with a weak normalization rationale, correlates more with the relative metrics on MuJoCo with tanh but more with the absolute metrics on ALE and MuJoCo with ReLU.

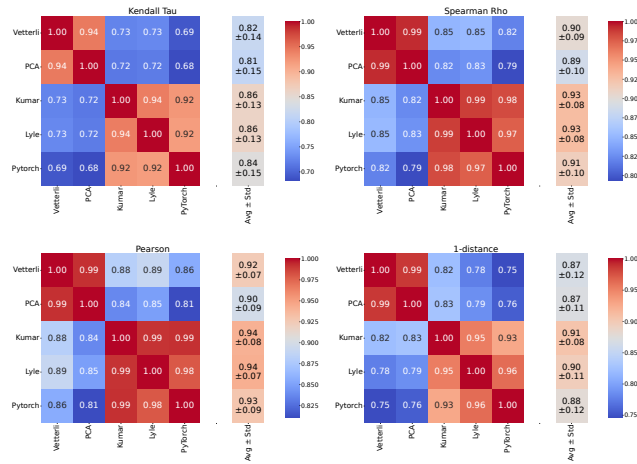


Figure 28: Average correlation between rank metrics on MuJoCo ALE.

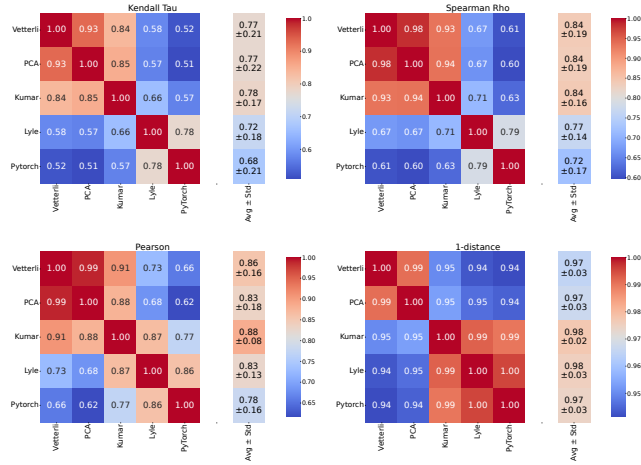


Figure 29: Average correlation between rank metrics on MuJoCo with the tanh activation.

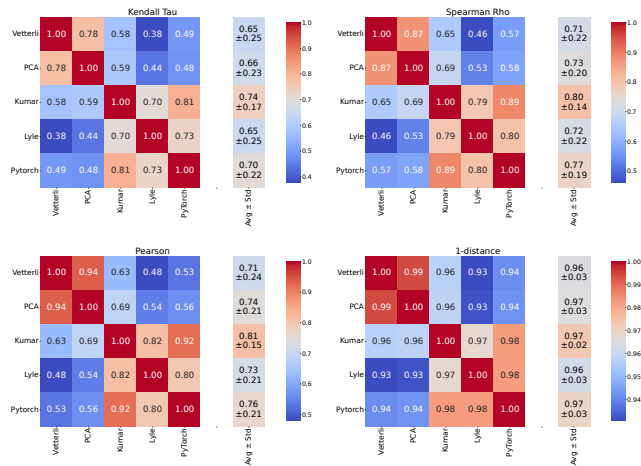


Figure 30: Average correlation between rank metrics on MuJoCo with the ReLU activation.

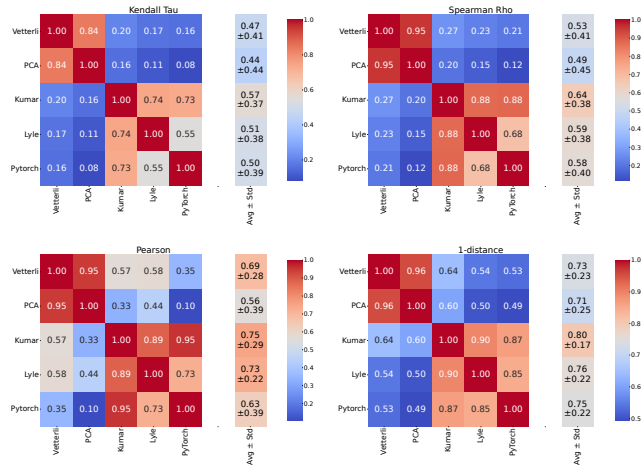


Figure 31: Worst-case correlations between rank metrics on ALE.

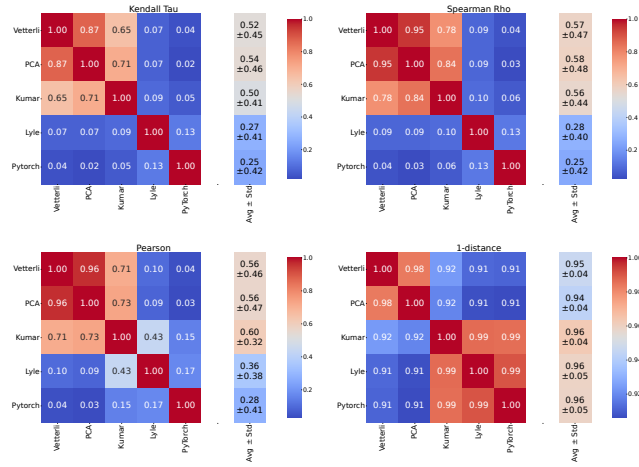


Figure 32: Worst-case correlations between rank metrics on MuJoCo with the tanh activation.

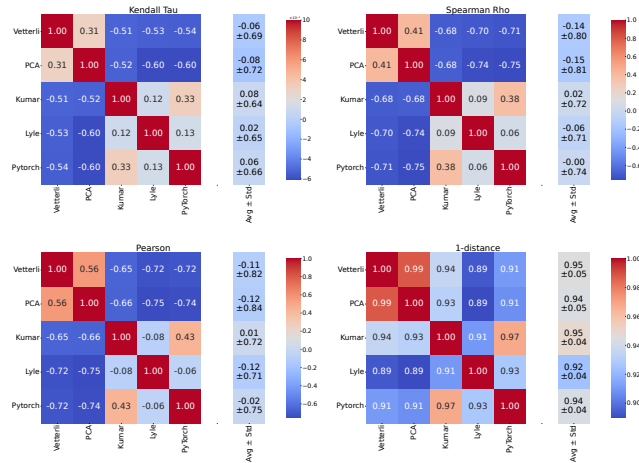


Figure 33: Worst-case correlations between rank metrics on MuJoCo with the ReLU activation.